Performance of MB-OFDM Ultra-Wideband Signals Over Fiber Transmission Using a Low Cost Electro-Absorption Modulator Integrated Laser

Chengwen Sui

A Thesis

In the Department

of

Electrical and Computer Engineering

Presented in Partial Fulfillment of the Requirements

For the Degree of Master of Applied Science at

Concordia University

Montréal, Québec, Canada

August 2010

Your file Votre référence
ISBN: 978-0-494-71054-8
Our file Notre référence
ISBN: 978-0-494-71054-8

ABSTRACT

Performance of MB-OFDM Ultra-Wideband Signals Over Fiber Transmission Using a Low Cost Electro-Absorption Modulator Integrated Laser

Chengwen Sui

The performance of multi-band (MB) orthogonal division frequency multiplexing (OFDM) ultra-wideband (UWB) over fiber transmission using a low cost electro-absorption modulator integrated laser (EML) is investigated in details. Various parameters such as fiber length, bias voltage, bias current and temperature of the EML are systematically evaluated to illustrate the effects on the performance of this Radio over Fiber (RoF) system. It is found that for the considered EML, the optimum normalized input (modulation) power is ~0.068 at bias voltage of 0.26 V. When modulation voltage is low the performance is mainly limited by signal to noise ratio, but mainly limited by EML response nonlinearities when modulation power is high.

Theoretical analysis of the effect of fiber dispersion and EML response nonlinearities on system performance is carried out considering amplitude and phase distortion. Experiments are conducted and verified by our theoretical analysis, and good agreement between the experiments is obtained. The effect of fiber chromatic dispersion induced laser phase to intensity noise conversion or relative intensity noise (RIN) on performance is investigated in terms of laser intrinsic RIN, laser linewidth, fiber dispersion and carrier frequency.

The effect of nonlinearities of the EML on the OFDM subcarriers for MB-OFDM UWB over fiber system is investigated in terms of the intermodulation distortion (IMD) products. In addition, adjacent channel power ratio (ACPR) is also analyzed and calculated in order to abide with ECMA standard and have less interference to coexisting channels.

Acknowledgements

First, I would like to express my sincere gratitude to my supervisor Dr. Xiupu Zhang for his guidance, advice, inspiration, and continuous support for me to finish this thesis.

I would also like to express my appreciation to Bouchaib Hraimel. Without his support and encouragement, I could not have finished this thesis. Also thanks to the folks at the Advanced Photonic System Lab for interesting discussions, and being fun to be with them.

I have sincere appreciation to the *Fonds de recherché sur la nature et les technologies (FQRNT)*, Quebec, Canada for supporting this research project.

Last but not least, I am very grateful to my father and mother for their continuous love and support throughout my life.

Table of Contents

List of Figures

List of Tables

List of Acronyms

ACPR	Adjacent Channel Power Ratio
ADS	Advanced Design System
AM/AM	Amplitude/ Amplitude
AM/ PM	Amplitude/ Phase
BPSK	Binary Phase Shift Keying
CTB	Composite Triple Beat Distortion
DC	Direct Current
DCF	Dispersion Compensating Fiber
DFB	Distributed Feedback
CATV	Cable Television
CW	Continuous Wave
EAM	Electro-Absorption Modulator
EBF	Electrical Bandpass Filter
ECMA	European Computer Manufacturers' Association
EDFA	Erbium Doped Fiber Amplifier
EIRP	Effective Isotropic Radiated Power
EML	Electro-Absorption Modulator integrated Laser
EVM	Error Vector Magnitude
FCC	Federal Communications Commission
FFT	Fast Fourier Transform

GVD	Group Velocity Dispersion
IFFT	Inverse Fast Fourier Transform
IMD	Intermodulation Distortion
LNA	Low Noise Amplifier
MAC	Multiple Access
MB	Multi-Band
MMF	Multi Mode Fiber
MZM	Mach-Zehnder Modulator
ODSB	Optical Double Side Band
O/E	Optical-to-Electrical
OFDM	Orthogonal Frequency Division Multiplexing
OSSB	Optical Single Side Band
OSA	Optical Spectrum Analyzer
PAPR	Peak to Average Power Ratio
PD	Photodetector
PER	Packet Error Rate
PHY	Physical Layer
PSD	Power Spectral Density
QAM	Qudrature Amplitude Modulation
QPSK	Quadrature Phase Shift keying
QoS	Quality of Service
RF	Radio Frequency
RIN	Relative Intensity Noise

RoF	Radio over Fiber
RS	Remote Station
SCM	Subcarrier Modulation
SFDR	Spurious-Free Dynamic Range
SMF	Single Mode Fiber
SNR	Signal to Noise Ratio
TFC	Time Frequency Code
UWB	Ultra wideband
WDM	Wavelength Division Multiplexing
WLAN	Wireless Access Networks
VA	Variable Attenuator
VOA	Variable Optical Attenuator
VCSEL	Vertical Cavity Surface Emitting Laser

List of Principal Symbols

A	Ampere
D	Dispersion Parameter ($ps/(nm \cdot km)$)
G_A	RF amplifier gain
f_c	RF carrier frequency
$I_k(\cdot)$	Modified Bessel function of the first kind of order
K	Boltzmann's Constant, $1.38 \cdot 10^{-23}$ J/K
L	Fiber length
N_{ST}	Number of subcarriers
$\Re$	Responsivity of the photodetector
s	Dispersion Slope ($ps/(nm^2 \cdot km)$)
T	Absolute Temperature
T_{CP}	Cyclic prefix (ns)
T_{GI}	Guard Interval
T_{FFT}	IFFT/FFT period

λ	Wavelength (nm)
ω	Frequency (TH_z)
$\Delta\omega$	Subcarrier spacing
β	Propagation Constant (radians/meter)
α	Fiber loss (dB/km)
β_2	GVD Coefficient (ps^2/km)
Δf	Subcarrier frequency spacing (MHz)
V_b	Bias voltage
V_m	Modulating signal voltage
V_{RF}	Driving voltage of the UWB signal

Chapter 1 Introduction

1.1 Background

Ultra-WideBand (UWB) radio communications are very attractive due to its promising capabilities to provide high data rate with low cost and low power consumption. The US Federal Communications Commission (FCC) authorized the use of the spectrum between 3.1 GHz and 10.6 GHz for UWB communications [1]. UWB signals are defined to occupy a frequency bandwidth of at least 500 MHz. The power spectral density (PSD) of emitted UWB must be as low as -41.3 dBm/MHz.

Low cost UWB wireless chips can be produced using CMOS technology. The chips should include all the front ends, filters, RF amplifiers, up/down mixers, analog to digital conversion/digital to analog conversion (ADC/DAC), and digital signal processing (DSP), which makes the design of UWB circuits in CMOS a challenging task. In fact, UWB is the first commercially available broadband OFDM wireless communication system.

At present, two major techniques are proposed for UWB communication. One is based on orthogonal frequency division multiplexing (OFDM) namely multi-band OFDM (MB-OFDM) and the other is based on very short duration pulses, namely impulse radio UWB (IR-UWB) pulses. In this thesis, the transmission of MB-OFDM signals over single mode fiber (SMF) is investigated.

Multiband-orthogonal frequency division multiplexing (MB-OFDM) has been proposed by the European Computer Manufacturer's Association (ECMA) [2] in December 2007. MB-OFDM becomes very attractive because it exhibits robustness in multipath fading environment, good spectral efficiency, high data rate capabilities between 53.5 and 480 Mb/s, and low power consumption. MB-OFDM divides the spectrum into six band groups and 14 sub-bands of 528 MHz bandwidth each [3]. Each OFDM symbol is composed of 128 orthogonal subcarriers spaced 4.125 MHz apart.

Due to low power, wide bandwidth and high frequency signals of the UWB, distribution of UWB over coaxial cable is very expensive. Optical fiber has low loss, low cost and wide bandwidth characteristics. One way to extend the range is to use radio over fiber (RoF) systems.

1.2 Radio over Fiber Technology

Radio over Fiber (RoF) a technology where light is modulated by a radio-frequency signal and transmitted over an optical fiber link. RoF is used for multiple purposes, such as in cable television (CATV) networks and in satellite base stations. Wireless networks based on RoF technologies have been proposed as a promising cost effective solution to meet the ever increasing user bandwidth and wireless demands.

RoF technology was developed by US Defense Advanced Research Projects Agency (DARPA) during early 1980s mainly for military applications. The purpose of the project was to place the radars and antennas far away from the command and control

centers due to the development of new radar-seeking missiles at that time. However, the technology has initially limited applications mainly due to high manufacturing cost of wide bandwidth lasers. In 1990, Cooper demonstrated the first fiber-radio system [4]. In his report, a four-channel, second-generation, cordless telephone system was demonstrated over single-mode fiber by using subcarrier multiplexing techniques. Since then, RoF systems and associated techniques have become an attractive topic for analog optical fiber communications and wireless communications. Different RoF techniques for present and future wireless communication systems have been reported.

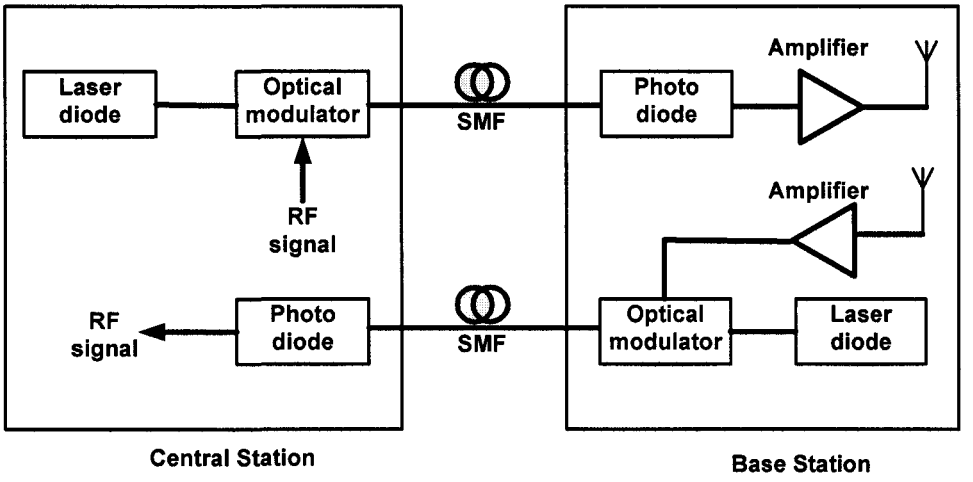

Figure 1.1 Basic RoF system.

Radio over fiber is an optical fiber link to distribute modulated RF signals from a central location to remote antenna units. RoF systems are usually composed of many base

stations (BSs), which are connected to a single central station (CS) as shown in Fig. 1.1. A basic RoF configuration consists of a two-way interface that contains a laser transmitter and photodiode receiver which connects the base station transmitters and receivers to a pair of single mode optical fibers. At the other end of the fibers is a remote unit that uses a similar photodiode receiver and laser transmitter to convert optical signals to and from an antenna. The main function of BS is to convert optical signal to wireless signal. Almost all processing including modulation, demodulation, coding, routing is performed at the CS.

1.2.1 Advantages of Radio over Fiber Systems

There are lots of advantages and benefits of the RoF distribution system, such as high bandwidth or high capacity of optical fiber, low attenuation, immunity to radio frequency interference, lower power consumption, and dynamic resource allocation are discussed below.

- **Low Attenuation**

Distributing high frequency radio signals electrically over long distances has high loss in free space and through transmission lines. RoF technology can be used to achieve both low loss distribution of RF signal, and simplification of RAUs at the same time. Single mode fibers (SMFs) made from silica have attenuation losses below 0.2 dB/km and 0.5 dB/km in the 1550 nm and the 1300 nm windows, respectively. These losses are much lower than the coaxial cable, whose losses are higher by three orders of magnitude at higher frequencies.

- **High Capacity**

Optical fibers offer large bandwidth. Optical fibers have three main transmission windows, which offer low attenuation for optical fiber: 850 nm, 1310 nm, and 1550 nm wavelengths. The combined bandwidth of the three windows for single mode fibers is more than 50 THz [5]. The commercially available optical systems utilize only a fraction of the high capacity (1.6 THz). The large bandwidth offered by optical fibers has benefits of high capacity for transmitting microwave signals as well as high speed signal processing in electronic systems. For example, some of the demanding microwave functions such as filtering, mixing, up and down conversion, can be implemented in the optical domain [6].

- **Immunity to Interference**

In optical fiber communication information is transmitted by modulating the light with RF signal. As a result Optical fiber has immunity to electro-magnetic interference. RoF does not suffer from multipath interference which is a common problem in normal wireless communication. Immunity to eavesdropping is another important characteristic of optical fiber. RoF provides privacy and security.

- **Low Power Consumption**

Simple remote antenna unit with reduced equipment leads low power consumption. Most of the complex equipment is kept at the centralized head end. In some applications, the remote antenna units are even operated in passive mode. Power consumption reduced at the remote antenna unit is a very important advantage.

- **Dynamic Capacity Allocation**

In RoF system, the allocate capacity is dynamic because of the switching, modulation, and other RF functions are performed at a centralized head end. Allocating capacity dynamically is needed for the desired requirements. Having the centralized head end facilitates the consolidation of other signal processing functions such as mobility functions, and macro diversity transmission [7].

1.2.2 Application of Radio over Fiber

The main application areas are briefly introduced as follows:

- **Cellular Networks**

Mobile traffic (e.g. CDMA, GSM, and UMTS) can be deployed simple and cost-effective between CSs and BSs via RoF system. RoF can also be applied to radio coverage extension in dense urban environments and capacity distribution and allocation [8].

- **CATV systems**

Fiber optical cable television (CATV) and RoF transport systems have recently been enhanced and implemented by the use of 1550 nm technology [9]. Fiber to home networks (FTTH) are used for multi point video distribution service (MVDS) and transmission of IEEE 802.16 broadband services.

- **Wireless Local Area Network (WLAN)**

RoF systems can be used for indoor distribution of wireless signals of both mobile and data communication (e.g. WLAN) systems. By using RoF technology, the capacity of optical networks can be combined with the flexibility and mobility of wireless access networks without significant cost increments. RoF can be applied to distribute WLAN signals operating at 2.4 GHz and 5 GHz.

- **Vehicle Communication and Control**

Road-vehicle communications and inter-vehicle communications play an essential role in Intelligent Transport Systems (ITS). Frequencies between 63 – 64 GHz and 76 – 77 GHz have been allocated for ITS in Europe. RoF extends the coverage of the road networks and makes ITS more manageable and effective.

1.3 Ultra-wideband Radio over Fiber

Ultra-wideband (UWB) radio over fiber is a novel technology in the field of short-range communication applications. UWB is an impulse radio standard that uses low power and a very wideband bandwidth (typically > 500 MHz), has been developed for short reach systems. The UWB radio signal is in the range of 3.1 – 10.6 GHz. Similar to RoF, UWB radio over fiber technology allows separation of low cost Base Stations (BS) from the Central Station (CS). The main differences between UWB radio over fiber and the conventional RoF are [10]:

- In the RoF technology, which targets the 2G/3G cellular systems, the RF signal bandwidth is only few 10's of MHz and its average power is in the range of

several 100 mW. This requires high cost photonic components in the CS and medium cost components in the BS.

- UWB radio over fiber is targeting the Personal Area Network (PAN) market that is characterized by very low cost and low power (10's μW) access point. In UWB radio over fiber, the optical fiber is used to carry extremely wide RF signals (several GHz).

An overview of UWB wireless technology is presented in Chapter 2.

1.4 Review of Relative Technologies and Motivation

Ultra-Wide Band (UWB) wireless technologies are very attractive due to its short range and high data rates. Radio over fiber (RoF) technology is a cost effective way to distribute UWB signals over long distances. The field is relatively new and there are many publications on UWB over fiber these years.

In recent years, many investigation of UWB signals transmission have been carried out, such as research on UWB based on pulse radios [11], UWB over fiber [12-15]. But MB-OFDM UWB signals are different from pulse radio UWB signal. Due to the high data rate between 53.3 Mbps to 480 Mbps, the distance of coverage is expected to be no more than a few meters. Many efforts have been made to explore the use of MB-OFDM UWB over long distance transmission for high data rate. In October 2006, Y. Guennec, et al, first investigated the distribution and processing of MB-OFDM UWB signals for radio over fiber network [16]. A. Pizzinat, et al., found that the performances

of a UWB OFDM system over fiber based on laser direct modulation are mainly limited by nonlinearities in the laser response [17]. Distribution of UWB wireless over SMF was also studied by M. Yee, et al. [18]. In September 2007, Y. Guo, et al., presented the packet error rate (PER) of MB-OFDM UWB signal transmission through multimode fiber based on radio over fiber system [19]. In an article published in IEEE International Microwave Symposium in May 2008, M. Lee, et al., investigated the performance of a WLAN over fiber system with band group 1 (3.168 ~ 4.752 GHz) of UWB [20]. In May 2009, bidirectional MB-OFDM UWB signal transmission through cable system, MMF and SMF based on RoF system was studied by M. L. Yee, et al. [21]. The results showed that the PER degrades quickly above 1 km transmission of multimode fiber (MMF) and the low loss characteristics of single mode fiber (SMF) enables the transmission distance of the UWB signals to be greatly extended. All these experiments were performed in directly modulation.

In August 2008, M. Jazayerifar, et al., investigated the performance of both MB-OFDM and IR-UWB transmission over SMF using distributed feedback (DFB) laser diode and Mach-Zehnder modulator (MZM) [22]. The first experimental demonstration of a bi-directional, reflective, electro-absorption transducer-based, 480 Mbps UWB-wireless/optical radio over fiber transmission system was presented in [23]. It was observed an EVM of -21.4 dB over 1 km of single mode fiber. Recently, the combined effects of fiber dispersion, and nonlinearities of optical transmitter's and optical receiver's response on the OFDM subcarriers for MB-OFDM UWB over fiber system using an MZM was studied by M. Sakib, et al. [24]. There are still many areas of UWB over fiber transmission yet to be covered.

An MZM usually has a well characterized and stable optical transfer curve. The electro-absorption modulator (EAM) was not extensively investigated for analog applications as compared with directly modulated laser diodes and Mach-Zehnder modulators (MZM), because the EAMs have complex transfer function that introduce high distortion characteristics.

An EAM is generally integrated with a DFB laser to form an electro-absorption modulated laser (EML). Monolithic integration of a laser diode (LD) and an EAM is very attractive as a transmitter module in an optical fiber communication system for its low-cost packaging due to its large spot size which is well matched to that of a single-mode fiber (SMF).

The objective of this thesis is to investigate the performance of MB-OFDM UWB signals over fiber transmission using a low cost electro-absorption modulator integrated laser (EML).

1.5 Thesis Scope and Contributions

In this thesis, for the first time to our knowledge, the performance of received MB-OFDM UWB signal over single mode fiber transmission using a low cost Electro-Absorption Modulator (EAM) integrated laser (EML) is investigated. Experiments are conducted to verify our theoretical analysis. The main contributions of this thesis are:

- The performance of MB-OFDM UWB over fiber transmission using an EML is investigated in details. Various parameters such as fiber length, bias voltage, bias

current and temperature of the EML are systematically evaluated to illustrate the effects on the performance of this RoF system.

- Theoretical analysis of the effect of fiber dispersion and EML response nonlinearities on system performance is carried out considering amplitude and phase distortion. Experiments are conducted and verified by our theoretical analysis and good agreement is obtained.

- The effect of fiber chromatic dispersion induced laser phase to intensity noise conversion or relative intensity noise (RIN) on performance is investigated in terms of laser intrinsic RIN, laser linewidth, fiber dispersion and carrier frequency.

- The effect of nonlinearities of the EML on the OFDM subcarriers for MB-OFDM UWB over fiber system is investigated in terms of the intermodulation distortion (IMD) products. In addition, adjacent channel power ratio (ACPR) is also analyzed and calculated in order to abide with ECMA standard and have less interference to coexisting channels.

1.6 Thesis Outline

The objective of this research work is to develop a UWB over fiber system that will ensure best performance and will provide economic solution to this fast growing technology. The rest of the thesis is organized as follows.

Chapter 2 presents an overview of UWB wireless technology, its advantages and real world applications. This chapter focuses on key aspects of MB-OFDM UWB with focus on IEEE 802.15.3 draft and ECMA-368 standard. The current frequency bands and standardization issues are also discussed. Basic mathematical framework and physical layer structure is described.

Chapter 3 presents an overview of EAM, the nonlinear characteristic transmission of the EAM is discussed. The measured characteristics of the EML versus EML bias voltage, bias current, and temperature are given.

Theoretical analyses are given in Chapter 4 considering carrier phase noise and fiber chromatic dispersion effect on each of the OFDM subcarriers within one symbol. The chapter also presents a simple approximation of the OFDM signal to derive a closed-form expression for the output spectrum.

Chapter 5 presents experimental setup for the performance evaluation of UWB over fiber system and two-tone test. The performance of UWB over fiber system is clarified with focus on the ECMA-368 standard using MB-OFDM. Error Vector Magnitude (EVM) measurement is carried out to evaluate the system performance considering the effect of fiber length, bias voltage, bias current, temperature, and input RF power of the EML. Optical transmitter's nonlinearities and fiber dispersion effect on system performance are studied experimentally and compared to the theoretical analysis.

In Chapter 6, the conclusions of this thesis are drawn, and a recommendation for the future work is proposed.

Chapter 2 UWB Overview

Ultra-wideband (UWB) systems have attracted a lot of attention in recent years. They have been popularized as a technology for short-range, high data rate communication and location applications. This chapter presents an overview of UWB wireless technology. This chapter focused on MB-OFDM UWB from IEEE 802.15.3 draft and ECMA-368 standard relevant to our research in UWB radio over fiber technology. The current frequency bands and standardization issues are also discussed. Basic mathematical framework and physical layer structure are described.

2.1 UWB Basics

Before UWB, the spectrum was divided up by frequency and only a very restricted overlap of authorized services was allowed. By contract, UWB is intentionally designed to overlap a broad swath of other services. Fig. 2.1 illustrates the relative power and bandwidth of UWB signal compared with the narrowband signals.

UWB started life in the late 1960s as a military technology radar which was capable of penetrating leaves and other foliage and used for covert communications. In this application, the military took advantage of the fact that UWB signals were spread across a very wide bandwidth and could be made to appear as noise to most interception equipment. In 1973, the first UWB communications patent was awarded for a short-pulse

receiver [25]. Through the late 1980s, UWB theory, techniques, and many implementation approaches had been developed for a wide range of applications, such as radar, communications, automobile collision avoidance, positioning systems, liquid-level sensing, and altimetry. By the late 1990s, UWB technology had become more commercialized and its development had accelerated greatly.

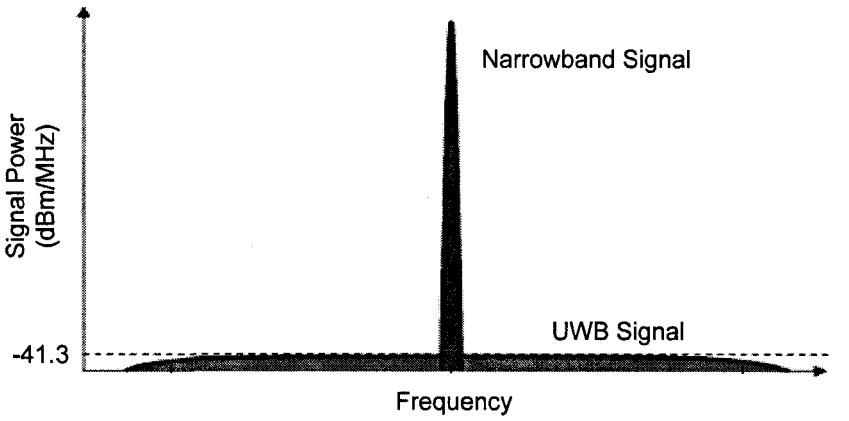

Figure 2.1 Power level of UWB signal and a typical narrowband signal

A substantial change in UWB history occurred in February 2002, U.S. Federal Communications Communication (FCC) issued UWB rulings that provided the first radiation limitations for UWB transmission [1]. The FCC has mandated that UWB radio transmission can legally operate in the range 3.1 to 10.6 GHz, with the power spectral density (PSD) satisfying a specific spectral mask. The spectrum allocation and power spectral mask required by FCC is shown in Fig. 2.2. The PSD of a UWB signal

transmitter power must not exceed -41.3 dBm/MHz. The current worldwide regulation for UWB is presented in Fig. 2.3.

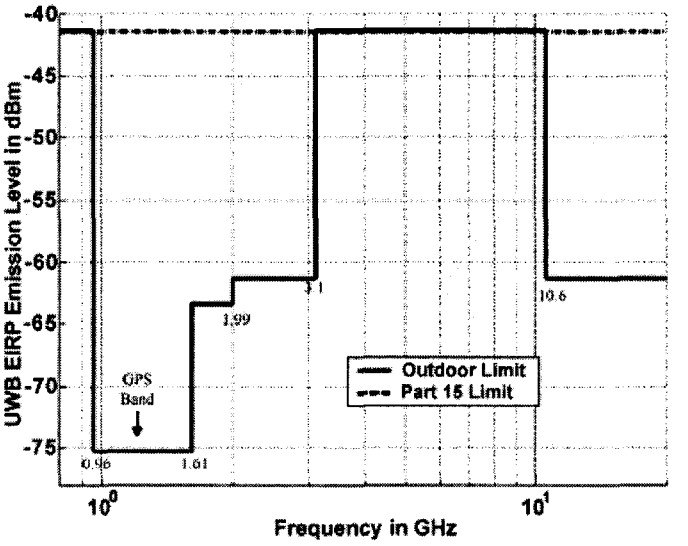

Figure 2.2 FCC UWB emission spectrum [1].

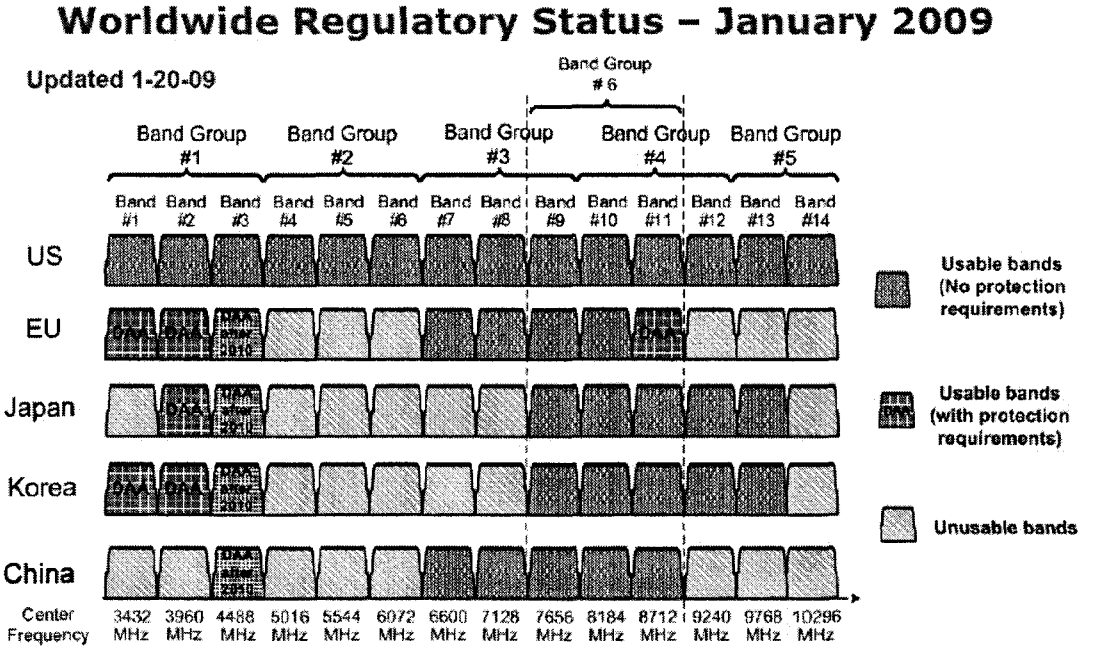

Figure 2.3 Current worldwide regulation for UWB [26]

2.2 UWB Applications

Due to its high capacity, low power and low cost, fading robustness and flexibility, UWB technology enables a wide variety of applications in wireless communications, networking, radar imaging, and localization systems. Examples of such technologies that could use the wireless flexibility or the high throughput offered by the UWB are:

- USB
- IP and related upper layers (TCP, DLNA, UPnP, etc.)
- Bluetooth
- FireWire (IEEE 1394)
- Home networking without physical connections
- Radio Frequency Identification (RFID) devices

2.3 MB-OFDM UWB

In the multiband OFDM proposal for IEEE 802.15.3a WPAN standard [3], the UWB signal occupies 512 MHz of bandwidth, allowing 14 signals to cover the entire 7.5 GHz band, as shown in Fig. 2.3. Each 528 MHz band uses OFDM, which allows each UWB band to be divided into a set of orthogonal narrowband channels.

The MB-OFDM signal consists of 128 subcarriers, and quadrature phase shift keying (QPSK) is used to modulate the transmitter signal at the subcarriers for the bit rate of 200 Mb/s and lower. Fig. 2.4 (a) shows RF spectrum for the first three-band of the 14 bands with bit rate of 200 Mb/s for each band, and the three bands are centered at frequency of f_1 = 3.432, f_2 = 3.96 and f_3 = 4.488 GHz. The signal follows simple frequency hoping sequences like f_1, f_2 and f_3 as shown in Fig. 2.4 (b) that is the spectrogram. Fig. 2.4 (c) shows the three bands in the time domain.

A MB-OFDM scheme is used to transmit information. A total of 110 sub-carriers (100 data carriers and 10 guard carriers) are used per band. In addition, 12 pilot subcarriers allow for coherent detection. Frequency-domain spreading, time-domain spreading, and forward error correction (FEC) coding are provided for optimum performance under a variety of channel conditions. A list of the timing parameters associated with the MB-OFDM PHY is listed in Table 2.1.

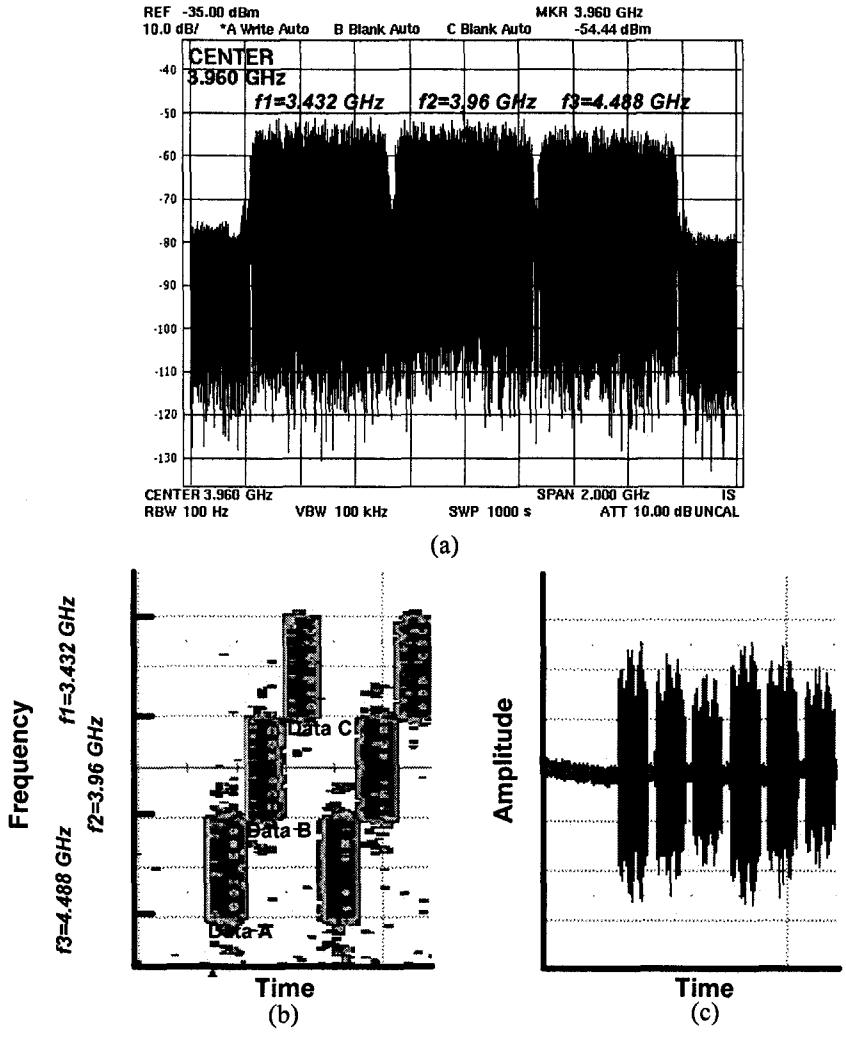

Figure 2.4 First three channels of MB-OFDM UWB wireless in (a) frequency domain, (b) frequency-time domain, and (c) time domain.

Table 2.1 Timing-related parameters of MB-OFDM [3]

Parameter	Description	Value
f_s	Sampling frequency	528 MHz
N_{FFT}	Total number of subcarriers (FFT size)	128
N_D	Number of data subcarriers	100
N_P	Number of pilot subcarriers	12
N_G	Number of guard subcarriers	10
N_T	Total number of subcarriers used	122 ($= N_D + N_P + N_G$)
D_f	Subcarrier frequency spacing	4,125 MHz ($= f_s / N_{FFT}$)
T_{FFT}	IFFT and FFT period	242,42 ns ($=1/\Delta f$)
T_{CP}	Cyclic prefix duration	60.61 ns(= 32/528 MHz)
T_{GI}	Guard interval duration	9.47 ns (= 5/528 MHz)
T_{SYM}	Symbol interval	312.5 ns ($T_{CP}+T_{FFT}+T_{GI}$)

2.3.1 MB-OFDM UWB Wireless Transmitter and Receiver

The structure of an MB-OFDM UWB transmitter and receiver is shown in Fig. 2.5. At the transmitter, the input data stream is first scrambled. The purpose of the data scrambler is to convert a data bit sequence into pseudorandom sequence that is free from long strings of simple patterns such as ones and zeroes. Then the data is conventionally encoded which improves the signal to noise ratio (SNR) due to addition of patterns of redundancy. The basic coding rate is usually called mother encoding rate. To obtain other coding rates, the coded sequence is again punctured. Puncturing is a procedure for omitting some encoded bits at the transmitter and inserting dummy zero into the sequence

received at the receiver in place of the bits omitted. The next block in the UWB transmitter is the bit interleaver. Bit interleaver provides robustness against burst errors, which consists of a symbol interleaving followed by tone interleaving. Then the bit interleaved sequence is mapped into a sequence of QPSK symbols according to gray coded constellation.

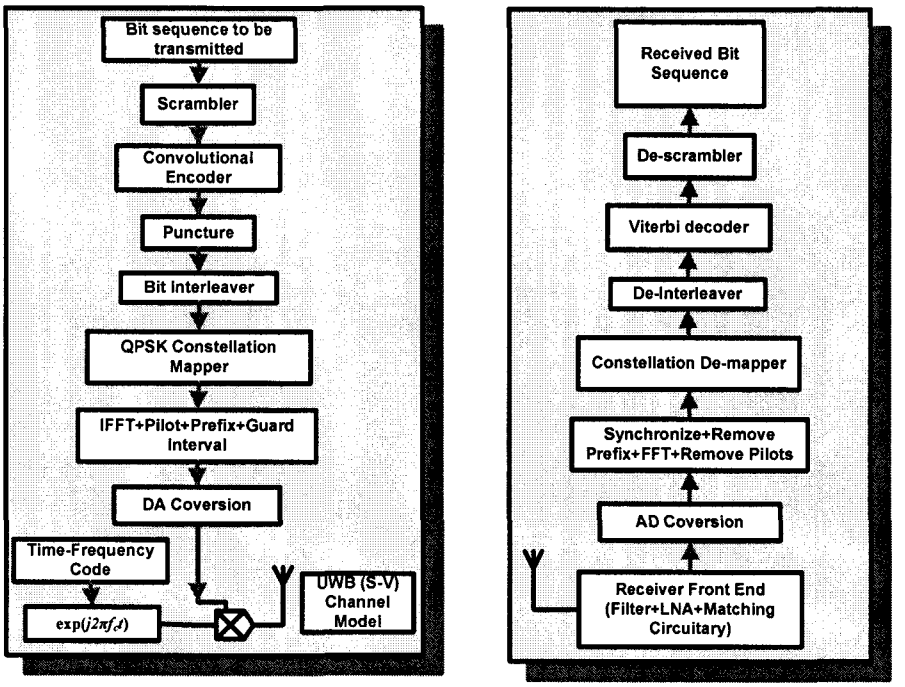

Figure 2.5 UWB transmitter and receiver [3].

2.3.2 Constellation Mapping

The OFDM subcarriers shall be modulated using QPSK modulation. The encoded and interleaved binary serical input data shall be divided into groups of 2 bits and converted

into complex numbers representing QPSK constellation points. The conversion shall be performed according to Gray-coded constellation mappings, illustrated in Fig. 2.6. The QPSK encoding table is shown in Table 2.2.

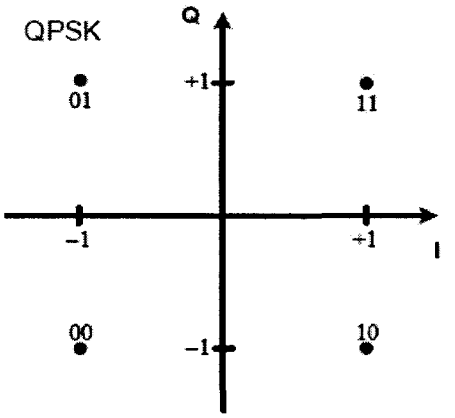

Figure 2.6 QPSK constellation [3]

Table 2.2 QPSK Encoding Table [3]

Input Bit	I-out	Q-out
00	-1	-1
01	-1	1
10	1	-1
11	1	1

2.3.4 Operating Band Frequencies

The relationship between center frequency and band number is given by the following equation:

$$\text{Band center frequency} = \begin{cases} 2904 + 528 \times n_b & n_b = 1 \ldots 4 \\ 3168 + 528 \times n_b & n_b = 5 \ldots 13 \end{cases} \quad (MHz)$$

This definition provides a unique numbering system for all channels that have a spacing of 528 MHz and lie within the band 3.1 – 10.6 GHz. Six band groups are defined in Fig. 2.7. Band groups 1 to 4 consist of 3 bands each, spanning the bands 1 to 12. Band group 5 contains the two bands 13 and 14. Band group 6 contains the bands 9, 10 and 11. The band allocation is summarized in Table 2.3.

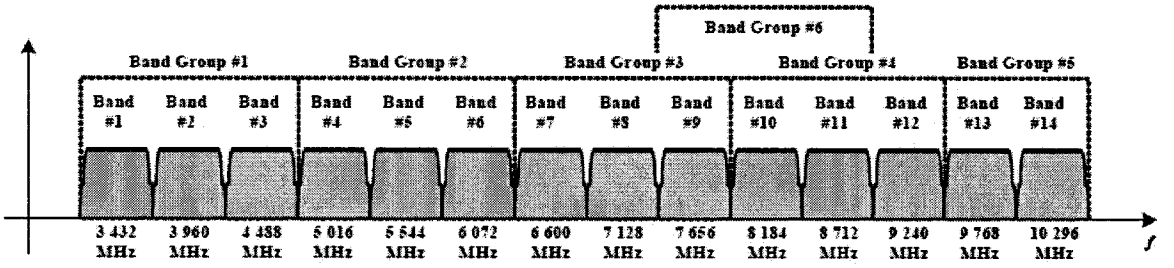

Figure 2.7 Diagram of the band group allocation [2].

Table 2.3 Band Group Allocation for MB-OFDM UWB [3]

Band Group	BAND ID	Lower Frequency (MHz)	Center Frequency (MHz)	Upper Frequency (MHz)
1	1	3168	3432	3696
	2	3696	3960	4224
	3	4224	4488	4752
2	4	4752	5016	5280
	5	5280	5544	5808
	6	5805	6072	6336
3	7	6336	6600	6864
	8	6864	7128	7392
	9	7392	7656	7920
4	10	7920	8184	8448
	11	8448	8712	8976
	12	8976	9240	9504
5	13	9504	9786	10032
	14	10032	10296	10560
6	9	7392	7656	7920
	10	7920	8184	8448
	11	8448	8712	8976

2.3.5 Rate-Dependent Parameters

The PSDU data rate-dependent modulation parameters are listed in Table 2.4.

Table 2.4 Data rate dependent Parameters for MB-OFDM system [3]

Data Rate (Mb/s)	Modulation	Coding Rate (R)	FDS	TDS	Coded Bits / 6 OFDM Symbol (N_{CBP6S})	Info Bits / 6 OFDM Symbol (N_{IBP6S})
53.3	QPSK	1/3	YES	YES	300	100
80	QPSK	1/2	YES	YES	300	150
106.7	QPSK	1/3	NO	YES	600	200
160	QPSK	1/2	NO	YES	600	300
200	QPSK	5/8	NO	YES	600	375
320	DCM	1/2	NO	NO	1200	600
400	DCM	5/8	NO	NO	1200	750
480	DCM	3/4	NO	NO	1200	900

2.3.6 Transmitter Constellation Error

The relative constellation RMS error, averaged over all data and pilot subcarriers of the OFDM symbols and over all of the frames, shall not exceed the values given in Table 2.5. The relative constellation error values are a function of the transmit power attenuation.

Table 2.5 Permissible Relative Constellation Error (EVM) [3]

	Relative Constellation RMS Error		
Data Rate	No TX Attenuation	TX Attenuation of 2, 4, 6 dB (All TFCs)	TX Attenuation of 8, 10, 12 dB (All TFCs)
53,3 Mb/s, 80 Mb/s, 106,7 Mb/s, 160 Mb/s, 200 Mb/s	−17,0 dB	-15,5 dB	-14,5 dB
320 Mb/s, 400 Mb/s, 480 Mb/s	−19,5 dB	-18,0 dB	-17,0 dB

2.4 Mathematical Description of MB-OFDM UWB Signal

The MB-OFDM RF signal $y_{RF}(t)$ is related to the complex baseband signal $x_k(t)$ of the k^{th} OFDM symbol as [3]

$$y_{RF}(t) = \mathrm{Re}\left\{\sum_{k=0}^{N-1} x_k(t - kT_{SYM})\exp(j2\pi f_c t)\right\} \tag{2.1}$$

where $\mathrm{Re}(\cdot)$ represents the real part of a complex variable, $x_k(t)$ is the complex baseband signal of the k^{th} OFDM symbol and is nonzero over the interval from 0 to T_{SYM}, N is the

number of OFDM symbols, T_{SYM} is the symbol interval, and f_c is the center frequency for the k^{th} band.

The OFDM symbols $x_k(t)$ can be constructed using inverse Fast Fourier transform (IFFT) with a certain coefficients C_n, which can consist of data symbols, pilots, and training symbols:

$$x_k(t) = \begin{cases} 0 & t \in [0, T_{CP}] \\ \sum_{n=-N_{ST}/2}^{N_{ST}/2} C_n \exp(j2\pi n\Delta f)(t - T_{CP}) & t \in [T_{CP}, T_{FFT} + T_{CP}] \\ 0 & t \in [T_{FFT} + T_{CP}, T_{FFT} + T_{CP} + T_{GI}] \end{cases} \quad (2.2)$$

where $N_{ST} = 128$ is the total number of subcarrier used, $\Delta f = BW / N = 4.125$ MHz is the subcarrier frequency spacing, n is the subcarrier number, $T_{CP} = 60.61$ ns is the cyclic prefix, $T_{FFT} = 1/\Delta f = 242.42$ ns is the IFFT/FFT period, and BW is the signal bandwidth.

Chapter 3 Characterization of Electro-Absorption Modulators Integrated Laser

In the later experiment, we investigate the performance of received MB-OFDM UWB signal over fiber transmission using a low cost Electro-Absorption Modulator (EAM) integrated Laser (EML). This chapter first begins with a brief overview of EAM. Then the nonlinearity of EAM is discussed. The measurements of the EML characteristics are given, and the absorption curves are used to extract extinction characteristics.

3.1 Introduction

Among telecommunication systems, transmitters and receivers act as interfaces between data processing and propagation media. For the optical transmitter, an electro/optical (E/O) converter is an optical modulator, which is used to convert the electric signal with a carrier frequency into optical format. Optical modulators are important components for long-haul, high bit rate optical communications. Optical modulators can be divided into two categories: electrooptic modulator and electro-absorption modulator (EAM). Mach-Zehnder modulator (MZM) is based on electrooptic effect. By modulating the electric field applied to one or both arm of an MZM, an index change is induced that causes the phase modulation. MZMs are widely used commercialized modulators.

An EAM is a semiconductor device which can be used for controlling (modulating) the intensity of a laser beam via an electric voltage. The EAM is a reverse-biased p-i-n diode with bulk active region or multiple quantum wells (MQWs) as the absorption layer and works on the principle of Franz-Keldysh effect. Compared with $LiNbO_3$-based MZM, the EAM waveguides are much shorter, which are ranging from 50 μm to 1 mm. Another advantage of EAM is higher modulation efficiency. For a bandwidth around 10 – 20 GHz, EAM can operate with much lower voltage. The V_π of an EAM is around 1~3 V, and the typical V_π of an MZM is 3~5 V. An EAM takes advantage of its small size, low driving voltage, low chirp and high bandwidth due to its inherent characteristics. A comparison of EAM and $LiNbO_3$ MZM is given in Table 3.1.

Table 3.1 Comparison of EAM and $LiNbO_3$ MZM [27]

	$LiNbO_3$ MZM	**EAM**
Cost	High (production process)	Potentially low
Power consumption	High drive voltage	Half drive voltage of $LiNbO_3$ MZM for same extinction ratio
Insertion loss	5 – 6 dB wavelength transparent	6 – 15 dB increase to low wavelength
Polarization dependency	Yes	Can be independent
Optical input power	High damage level	Max. ~ 10-12 dBm mean
Chirp	Different chirp for raising and falling part. Zero chirp available	Low chirp available
Extinction ratio	Typically ~ 15 dB	High, > 30dB reported decrease to long wavelength
Bandwidth	~ 45 GHz	> 50 GHz
Pulse carving	33, 50 or 66% duty cycle not suitable for OTDM	10-20% possible with high dynamic extinction ratio

In addition, due to matching of material systems, EAM can be easily integrated with other optical components, such as semiconductor lasers, semiconductor optical amplifiers, and attenuators. Electro-absorption modulator integrated Laser (EML) is one type of low cost optical transmitter. The EML is an EAM integrated with a laser diode on the same chip, has been commercially available for a long time. However, an EML has a complex nonlinear transfer function that introduces intermodulation distortion (IMD) when optical subcarrier modulation is used. IMD will degrade and limit the transmission performance of RoF link. Two-tone test is a convenient way to measure IMD in simple modulation schemes. Adjacent channel power ratio (ACPR) is the logical extension of the distortion measurement except that the two tones are replaced by a given modulated signal [28]. ACPR can denote the interference power to existing systems in the adjacent channels as well as the loss of the available amplifier output power.

3.2 Nonlinearities of EAM

The nonlinearity issue in RoF mainly comes from the optical modulator and chromatic dispersion of the optical fiber. Compared to the direct modulation scheme, the main drawbacks of external modulation are more expensive and the additional optical insertion loss introduced by the modulator. Semiconductor lasers feature output optical intensity proportional to the drive current, and hence modulation of the drive current produces direct modulation of the optical signal. An MZM usually has a well characterized and stable optical transfer curve. In contrast, the optical transfer curve of an EAM is dependent on both material properties and the device structure and cannot be easily

described analytically. Therefore, it becomes very complicated to employ similar schemes to linearize an EAM link.

The EAM introduces the non-linearity to the link, because the relation between the electrical input and the optical output of the EAM is not linear. The transfer function of the EAM is represented as follows [29]:

$$P_{out}(V) = P_{in} \exp\left[-\Gamma \alpha(V) L\right] = T(V) \tag{3.1}$$

where P_{in} is the input optical power of EAM, Γ is the confinement factor, α is the absorption coefficient, and L is the length of the EAM. Among these variables, it is important to obtain the absorption coefficient as a function of dc bias voltage in order to find the transfer function of the EAM. Fig. 3.1 shows the normalized power transfer function for the EAM.

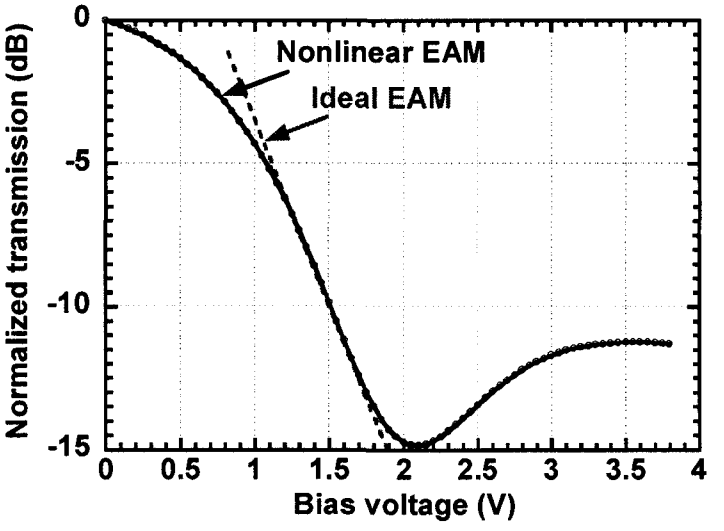

Figure 3.1 Normalized transmission versus bias voltage for the EAM

The non-linearity generates new frequency components at the RF output. Using a small-signal approximation, the harmonic and intermodulation distortions of the RF signals after passing the EAM can be evaluated by expanding its transfer function using a Taylor series. When the modulator is biased at DC voltage V_b and a modulating voltage V_m, the total applied voltage becomes $V = V_b + V_m$, and Eq. (3.1) can be represented as follows [9]

$$\begin{aligned}\frac{P_{out}}{P_{in}}(V) &= T(V) \\ &= T(V_b) + V_m \left.\frac{dT}{dV}\right|_{V_b} + V_m^2 \frac{1}{2!}\left.\frac{d^2T}{dV^2}\right|_{V_b} + V_m^3 \frac{1}{3!}\left.\frac{d^3T}{dV^3}\right|_{V_b} + \cdots \\ &= K_0 + K_1 V_m + K_2 {V_m}^2 + K_3 {V_m}^3 + \cdots\end{aligned} \tag{3.2}$$

where K_0, K_1, K_2, and K_3 are the Taylor series coefficients of the DC, first-order, second-order, and third-order component, respectively. When a two-tone signal of f_1 and f_2 is applied, the magnitude of the received RF signal of f_1 and f_2, the composite second-order distortion (CSO) of $f_1 \pm f_2$, and the composite triple-beat distortion (CTB) of $2f_1 - f_2$ and $2f_2 - f_1$ can determine the link performance [10]. Second-order intermodulation distortion (IMD2) and third-order intermodulation distortion (IMD3) are dominated by the second and third derivatives of the transfer function of the EAM, which can be represented by Eqs. (3.3) and (3.4), respectively:

$$\text{IMD2} = 10\log_{10}\left[\frac{\sum f_1 \pm f_2\big|_{\text{power}}}{f_1 \text{ or } f_2\big|_{\text{power}}}\right] \tag{3.3}$$

$$\text{IMD3} = 10\log_{10}\left[\frac{\sum 2f_2 - f_1\big|_{\text{power}}}{f_2\big|_{\text{power}}}\right] \text{ or } 10\log_{10}\left[\frac{\sum 2f_1 - f_2\big|_{\text{power}}}{f_1\big|_{\text{power}}}\right] \tag{3.4}$$

If f_1 *and* f_2 are close, all the second order products will be far from f_1 or f_2, and can easily be filtered out from the output of the component. So the magnitude of the IMD3 products is the most important parameter in determining the link performance.

The nonlinearity of an EAM causes distortions and reduces the dynamic range of a radio frequency (RF) link. The nonlinear transfer function has a strong dependence on input optical wavelength and power, which could limit the dynamic range and the link gain of an RF link. Spurious-free Dynamic Range (SFDR) is an important figure of merit of an analog fiber-optic link. SFDR is the dynamic range of fundamental signal power to the power level when spurious distortions start to emerge above the output noise. For the most conventional links, SFDR is limited by IMD from the transfer function of the MZM or EAM, and by the high intensity noise associated with optical carrier power. SFDR is usually characterized by a two-tone test.

3.3 Electro-Absorption Modulator Integrated Laser

3.3.1 Schematic Structure of the EML

In the experiments, we used an electro-absorption modulator integrated laser (EML) instead of an EAM because the EML is less costly. Electro-absorption modulator integrated with a DFB-Laser diode is now a well-established technology for 2.5Gbit/s telecommunications of fiber optics where it tends to gradually replace the traditional lithium niobate modulator fed with a DFB-laser [10]. In this experiment, we used a 10 Gbit/s digital laser module with integrated electro-absorption modulator from Alcatel. A

view of 1915 LMM Alcatel module and the schematic view of EML Alcatel are shown in Fig. 3.2 (a) and 3.2 (b), respectively.

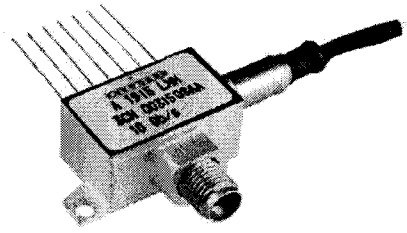

(a)

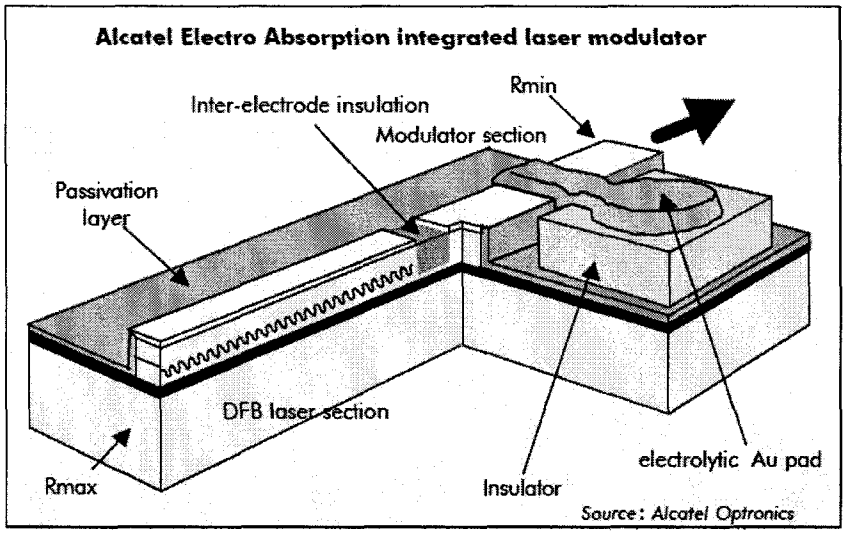

(b)

Figure 3.2 (a) View of 1915 LMM Alcatel module and (b) Schematic view of EML [30]

The modulation voltage is applied to the modulator section while the DFB laser operates CW. Without the complexity of $LiNbO_3$ external modulators, the Alcatel 1915

LMM is dedicated to STM64/OC-192 bit rate with reduced size and reduced cost. The device allows 10 Gbit/s data transmission with an extinction ratio higher than 10 dB and less than 2 V modulation voltage.

3.3.2 Device Characteristics

In this section, the measured characteristics of the EML are given. It is well known that lasers can survive wide range of temperature, on which their characteristics are dependent, such as peak emission wavelength and threshold current change. Fig. 3.3 shows the wavelength dependence of the temperature at laser bias current of 40, 60, 80 and 100 mA. As indicated in Fig. 3.3, the laser wavelength depends linearly on temperature with the same slope. The slope of the curves is equal to the temperature sensitivity. We can observe that the temperature sensitivity is ~0.1 nm/ °C in the temperature range of 20 to 55 °C.

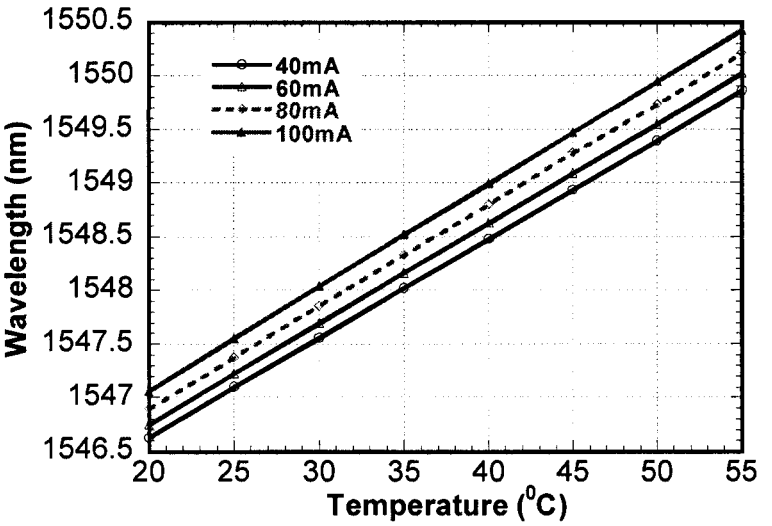

Figure 3.3 Laser wavelength versus temperature at different laser bias current.

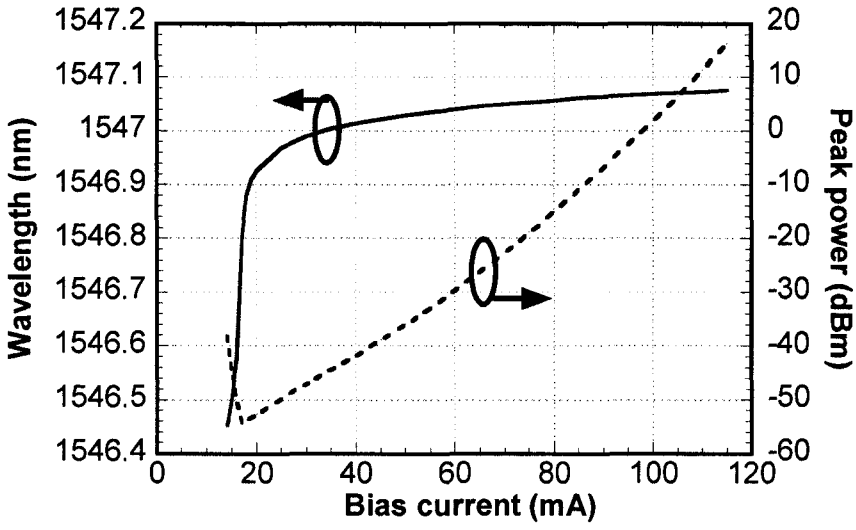

Figure 3.4 Wavelength and peak power versus Laser bias current at 25 °C.

Fig 3.4 shows the wavelength and peak power versus Laser bias current at 25 °C. From Fig. 3.4, it can be seen that with an increase of the bias current, the wavelength is increased, and the peak power is enhanced.

The EML optical output power is measured versus Laser bias current for temperature from 20 °C to 55 °C in steps of 5°C. Fig. 3.4 shows that the optical output power is approximately linear with respect to the current above the threshold current and decreases as the temperature increases. From Fig. 3.4 (a), it is observed that the threshold current increases as the temperature increases as shown in Fig. 3.4 (b).

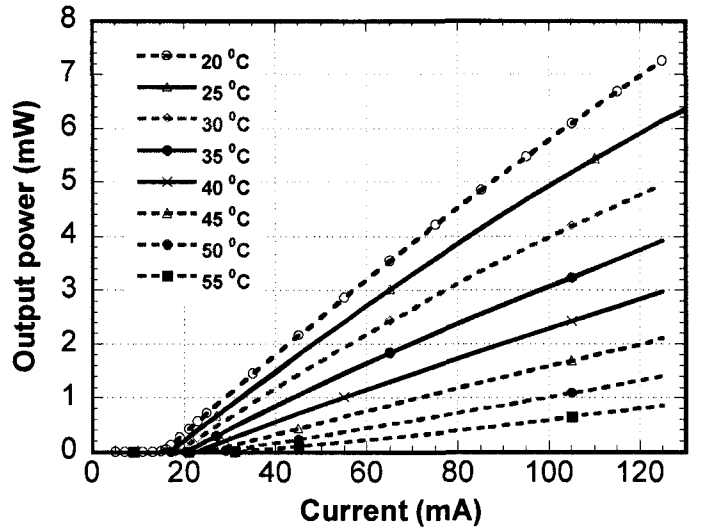

(a)

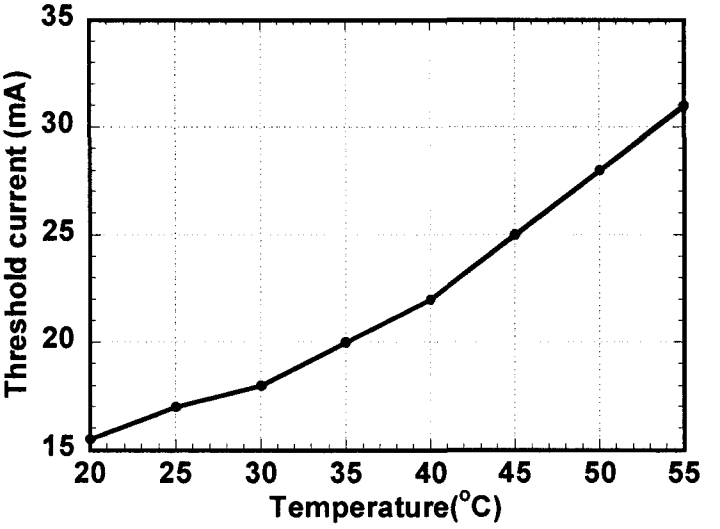

(b)

Figure 3.5 (a) EML output power versus laser bias current at different temperatures. (b) Threshold current versus temperature.

Next, we changed the DC bias voltage of the EML from 0 – 3 V, by the step of 0.05 V, and measured the optical power after every time we change the DC bias voltage of the EAM. The measured normalized power versus EML bias voltage at a Laser bias

current of 80 mA from 20 °C to 60 °C in steps of 5 °C is shown in Fig. 3.5. It is shown that the EML transfer function is dependent on temperature. It is observed that the transfer function linearity becomes worst and the extinction ratio degrades as the temperature increases. This is because at higher temperature, the residual optical absorption due to the interband absorption is larger. The extinction curve shifts to lower voltages due to the reduced detuning between modulator and laser source wavelength [31].

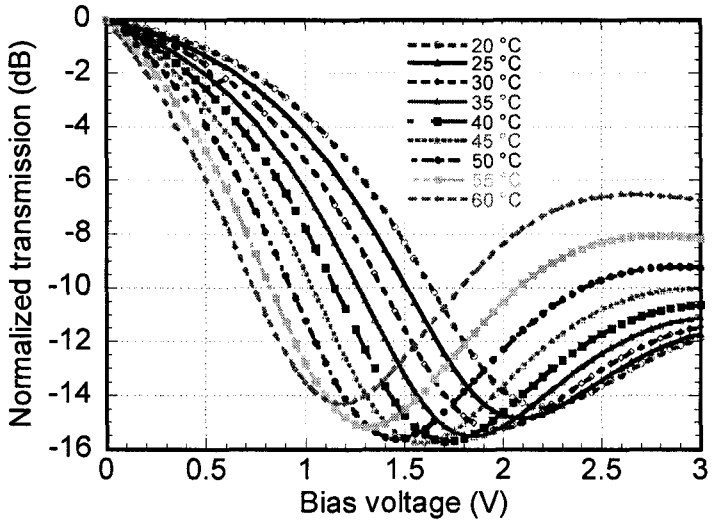

Figure 3.6 Measured relative transmission characteristics of the EML at different temperatures. The laser bias current is 80 mA.

3.4 Summary

This chapter gives a brief overview of EAM. Then the nonlinearity of EAM is discussed. Also the measured characteristics of the EML versus EML bias voltage, bias current, and temperature are given, and the absorption curves are used to extract extinction characteristics.

Chapter 4 Theoretical Analysis

In this chapter, theoretical analysis is carried out considering EML nonlinearities (IMDs and ACPRs), fiber chromatic dispersion and laser relative intensity noise (RIN).

First of all, the transfer function characteristic is extracted as shown in Fig. 3.5 at 25 °C. A seventh-order polynomial fitting of the transfer function of the EML is expressed by

$$\begin{aligned} T(V)|_{dB} = &-0.20391 + 4.6591V - 38.577V^2 + 81.828V^3 \\ &-86.701V^4 + 44.705V^5 - 10.88V^6 + 1.0075V^7 \end{aligned} \tag{4.1}$$

where V is the bias voltage of the EML. Note reverse voltage is included already in (4.1) and thus the positive voltage V is used in the rest of the contexts. We can convert a decibel (dB) scale into a linear scale, and (4.1) can be written as

$$T(V) = 10^{\frac{1}{10}\left(-0.20391+4.6591V-38.577V^2+81.828V^3-86.701V^4+44.705V^5-10.88V^6+1.0075V^7\right)}$$

$$= \exp\left[\frac{\ln 10}{10}\begin{pmatrix} -0.20391 + 4.6591V - 38.577V^2 + 81.828V^3 \\ -86.701V^4 + 44.705V^5 - 10.88V^6 + 1.0075V^7 \end{pmatrix}\right] \tag{4.2}$$

The MB-OFDM UWB signal is applied to the EML to modulate a CW lightwave with an optical power P_{in} and a random phase ϕ_c at wavelength λ or frequency f_c. For the EML biased at DC voltage V_b and a modulating voltage V_m, the total applied voltage is given by $V = V_b + V_m$. The output optical field from the EML can be written as

$$E_{out}(t) = \sqrt{T(V)}\sqrt{2P_{in}} \cdot e^{j(2\pi f_c t + \phi_c)} \tag{4.3}$$

The transmitted MB-OFDM RF signal V_m can be written in terms of the complex baseband signal $x(t)$ as $V_m = V_{RF}\,\mathrm{Re}\left(x(t)e^{j(\omega_{RF}t+\varphi(t))}\right)$, where Re(·) represents the real part of the signal, V_{RF} is the driving voltage of the UWB signal, ω_{RF} is angular frequency of the RF carrier, and $\varphi(t)$ is the phase noise of RF carrier.

The OFDM symbol $x(t)$ can be constructed within one symbol period, using an inverse Fast Fourier transform (IFFT) with a certain coefficient C_k, which consists of data, pilots, and training symbols, $x(t) = \sum_{n=-N_{ST}/2}^{N_{ST}/2} C_n \exp\left[j2\pi n\Delta f\left(t - T_{CP}\right)\right]$, $t \in \left[T_{CP}, T_{FFT} + T_{CP}\right]$, otherwise 0, where N_{ST} = 128 is the total number of subcarriers, $\Delta f = B / N_{ST} = 4.125$ MHz is the subcarrier frequency spacing, T_{CP} = 60.61 *ns* is the cyclic prefix, T_{FFT} = $1/\Delta f$ = 242.42 *ns* is the IFFT/FFT period, and B is the signal bandwidth. $C_n = |C_n|e^{j\theta_n}$ is the baseband QPSK signal at the n^{th} subcarrier.

4.1 Impact of EML Nonlinearities

In this section, the impact of the EML nonlinearity on each subcarrier of the OFDM symbol is studied. Fiber chromatic dispersion will not be considered here because the EML chirp is assumed to be negligible and will not interplay with fiber chromatic dispersion.

Substituting signal voltage $V = V_b + V_m$ into (4.3), after expansion in terms of trigonometric functions with combined arguments and considering only inter-symbol interference by ignoring all mixing products from different subcarriers, the optical field can be rewritten as

$$E_{out}(t) = \sqrt{2P_{in}} \cdot e^{j(2\pi f_c t + \phi_c)} \times \exp\left\{ \sum_{k=-N_{ST}/2}^{N_{ST}/2} \left[\begin{array}{l} \gamma_{0,k} + \gamma_{1,k} \cos\psi_k(t) + \gamma_{2,k} \cos 2\psi_k(t) \\ + \cdots + \gamma_{7,k} \cos 7\psi_k(t) \end{array} \right] \right\} \tag{4.4}$$

where $\gamma_{p,k}$ ($p = 0, \cdots, 7$ and $k = -N_{ST}/2, \cdots, N_{ST}/2$) depends on V_b , $|C_n|$, V_{RF} and the coefficients of the polynomial exponent of transfer function of the EML (given by (4.2)), and $\psi_k(t) = 2\pi k \Delta f (t - T_{CP}) + \omega_{RF} t + \theta_k + \varphi(t)$. Using Sonine's expansion

$$e^{z\cos\theta} = I_0(z) + 2\sum_{k=1}^{\infty} I_k(z) \cos k\theta = \sum_{k=-\infty}^{+\infty} I_k(z) e^{jk\theta} \tag{4.5}$$

where $I_k(\cdot)$ is the modified Bessel function of the first kind of order k, (4.4) can be reduced to

$$\begin{aligned} E_{out}(t) = \sqrt{2P_{in}} \cdot e^{j(2\pi f_c t + \phi_c)} \exp\left[\sum_{n=-N_{ST}/2}^{N_{ST}/2} \gamma_{0,n} \right] \\ \times \left(\sum_{n_{k_1}=-\infty}^{+\infty} \prod_{k_1=-N_{ST}/2}^{N_{ST}/2} I_{n_{k_1}}(\gamma_{1,k_1}) e^{j \sum_{k_1=-N_{ST}/2}^{N_{ST}/2} n_{k_1}\psi_{k_1}(t)} \right) \\ \times \left(\sum_{n_{k_2}=-\infty}^{+\infty} \prod_{k_2=-N_{ST}/2}^{N_{ST}/2} I_{n_{k_2}}(\gamma_{2,k_2}) e^{j \sum_{k_2=-N_{ST}/2}^{N_{ST}/2} 2n_{k_2}\psi_{k_2}(t)} \right) \times \cdots \\ \times \left(\sum_{n_{k_7}=-\infty}^{+\infty} \prod_{k_7=-N_{ST}/2}^{N_{ST}/2} I_{n_{k_7}}(\gamma_{7,k_7}) e^{j \sum_{k_7=-N_{ST}/2}^{N_{ST}/2} 7n_{k_7}\psi_{k_7}(t)} \right) \end{aligned} \tag{4.6}$$

The optical field of the carrier and subcarrier at $\pm\omega_r$ ($\omega_r = \omega_{RF} + 2\pi r\Delta f$) can be expressed as

$$E_0(t) = \sqrt{2P_{in}} \cdot e^{j(2\pi f_c t + \phi_c)} \exp\left[\sum_{k=-N_{ST}/2}^{N_{ST}/2} \gamma_{0,k}\right] \tag{4.7a}$$

$$\begin{aligned} E_{\pm\omega_r}(t) = \sqrt{2P_{in}} \cdot e^{j(2\pi f_c t + \phi_c)} \exp\left[\sum_{k=-N_{ST}/2}^{N_{ST}/2} \gamma_{0,k}\right] \left\{\prod_{p=1}^{7}\left[\prod_{k_p=-N_{ST}/2}^{N_{ST}/2} I_0\left(\gamma_{p,k_p}\right)\right]\right\} \\ \times \begin{Bmatrix} a_1(\gamma_{1,r}) + a_1(\gamma_{2,r})a_1(\gamma_{3,r}) \\ + a_1(\gamma_{4,r})a_1(\gamma_{5,r}) + a_1(\gamma_{6,r})a_1(\gamma_{7,r}) \end{Bmatrix} e^{\pm j\psi_r(t)} \end{aligned} \tag{4.7b}$$

where $a_1\left(\gamma_{p,k_p}\right) = I_1\left(\gamma_{p,k_p}\right) / I_0\left(\gamma_{p,k_p}\right)$.

After photodetection and electrical filtering, the received r^{th} subcarrier current of the OFDM symbol can be expressed as

$$\begin{aligned} i_r(t) \infty \exp\left[2\sum_{k=-N_{ST}/2}^{N_{ST}/2} \gamma_{0,k}\right] \left\{\prod_{p=1}^{7}\left[\prod_{k_p=-N_{ST}/2}^{N_{ST}/2} I_0^2\left(\gamma_{p,k_p}\right)\right]\right\} \\ \times \begin{Bmatrix} a_1(\gamma_{1,r}) + a_1(\gamma_{2,r})a_1(\gamma_{3,r}) \\ + a_1(\gamma_{4,r})a_1(\gamma_{5,r}) + a_1(\gamma_{6,r})a_1(\gamma_{7,r}) \end{Bmatrix}^2 \end{aligned} \tag{4.8}$$

When the bias voltage of the EML is 0.26 V, the coefficient $\gamma_{p,k}$ ($p = 0, \cdots, 7$ and $k = -N_{ST}/2, \cdots, N_{ST}/2$) can be expressed by

$$\begin{aligned} \gamma_{0,k} &= -0.0585441 - 0.160052\left(V_{RF}|C_k|\right)^2 - 1.68364\left(V_{RF}|C_k|\right)^4 - 0.325469\left(V_{RF}|C_k|\right)^6 \\ \gamma_{1,k} &= -0.455403\left(V_{RF}|C_k|\right) + 1.57291\left(V_{RF}|C_k|\right)^3 + 2.09841\left(V_{RF}|C_k|\right)^5 + 0.0634335\left(V_{RF}|C_k|\right)^7 \\ \gamma_{2,k} &= -0.160052\left(V_{RF}|C_k|\right)^2 - 2.24485\left(V_{RF}|C_k|\right)^4 - 0.488203\left(V_{RF}|C_k|\right)^6 \\ \gamma_{3,k} &= 0.524303\left(V_{RF}|C_k|\right)^3 + 1.0492\left(V_{RF}|C_k|\right)^5 + 0.038061\left(V_{RF}|C_k|\right)^7 \end{aligned}$$

$$\gamma_{4,k} = -0.561213\left(V_{RF}\left|C_k\right|\right)^4 - 0.195281\left(V_{RF}\left|C_k\right|\right)^6$$
$$\gamma_{5,k} = 0.209841\left(V_{RF}\left|C_k\right|\right)^5 + 0.0126867\left(V_{RF}\left|C_k\right|\right)^7$$
$$\gamma_{6,k} = -0.0325469\left(V_{RF}\left|C_k\right|\right)^6$$
$$\gamma_{7,k} = 0.000181239\left(V_{RF}\left|C_k\right|\right)^7$$

Eq. (4.8) shows that each subcarrier will be distorted in the amplitude. This distortion results from intrinsic nonlinearities of the EML response.

Next, nonlinear distortion introduced by the EML is analyzed by expressing the power spectral density of the received RF signal. A complex baseband OFDM signal with a high number of subcarriers can be approximated by a complex Gaussian process. The magnitude distribution of the OFDM signal therefore has a Rayleigh distribution. The first-zone output autocorrelation $R_{yy}(\tau)$ of a memoryless nonlinear system can be expressed in terms of input signal autocorrelation $R_{xx}(\tau)$ as follows [32]

$$R_{yy}(\tau) = \sum_{k=0}^{\infty} c_k \left[\frac{R_{xx}(\tau)}{2\sigma^2}\right]^{2k+1} \tag{4.9}$$

where $2\sigma^2$ is the mean power of the input signal $V_{RF}\left|x(t)\right|$ and the coefficients d_k are calculated according to Eq. (7) in [33],

$$d_k = \frac{1}{2}(k+1)\left(\sum_{l=1}^{[N/2]} 2^l \alpha_l \sigma^{2(l-1)} \sum_{n=0}^{k} \frac{1}{n!}\binom{k}{n}(n+l)!\right)^2 \tag{4.10}$$

with $l = 2k+1$, where $\alpha_l = \frac{1}{2^{2l} l!(l-1)!} \times \frac{\partial^{(2l-1)} T(V)}{\partial v^{(2l-1)}}$ and $T(V)$ is the transfer function of the EML. The values of the coefficient d_k in (4.10) are outlined in Table 4.1.

The undistorted OFDM signal, when properly filtered or windowed, exhibits a rapid decaying spectrum outside the main spectrum region [32]. Therefore, the OFDM signal spectrum can be approximated by a rectangular function. We can get the closed form expression for the k-fold convolution of the rectangular function by taking the k^{th} power of the inverse Fourier transform of the rectangular function and then taking the Fourier transform. The spectrum of the k^{th} term can be written as the following expression

$$s_k(v)=\frac{2(2\sigma^2)^l}{2^l\pi^{(l-1)}(l-1)!}\sum_{m=0}^{l}(-1)^m\binom{l}{m}(v+l-2m)^{(l-1)}u(v+l-2m) \tag{4.11}$$

where v is the normalized frequency and $u(\cdot)$ is the Heaviside unit step function. With d_k given by (4.10), the approximate power spectral density (PSD) of the output signal can be expressed

$$S_y(v)=\sum_{k=0}^{\infty}d_k s_k(v) \tag{4.12}$$

For k = 0, 1 and 2, $d_0 s_0(v)$, $d_1 s_1(v)$ and $d_2 s_2(v)$ are the PSD of UWB signal, third-order IMD (IMD3) and the fifth-order IMD (IMD5), respectively. The IMD3 products are the most important in determining the link performance.

Using the above equations, the output PSD can be numerically calculated if the input autocorrelation or PSD is given. The PSD of a distorted OFDM signal as computed numerically using (4.10), (4.11) and (4.12) is shown in Fig. 4.1. The normalized frequency is defined by normalizing to $B/2$, and [-1, 1] is considered the desired in-band. Within the in-band area the spectrum is almost constant. Outside this band the spectrum

decreases, and it may cause relatively high out-of-band intermodulation distortion and interference to adjacent channels.

Table 4.1 Values of the coefficient d_k

k	l	d_k
0	1	$\frac{1}{2}\left(-0.256645-0.509829\sigma^2-4.03669\sigma^4-0.669585\sigma^6\right)^2$
1	3	$\left(-0.769936-2.03932\sigma^2-20.1834\sigma^4-4.01751\sigma^6\right)^2$
2	5	$\frac{3}{2}\left(-2.05316-6.62778\sigma^2-76.697\sigma^4-17.4092\sigma^6\right)^2$
3	7	$2\left(-5.13291-19.3735\sigma^2-254.311\sigma^4-64.2802\sigma^6\right)^2$

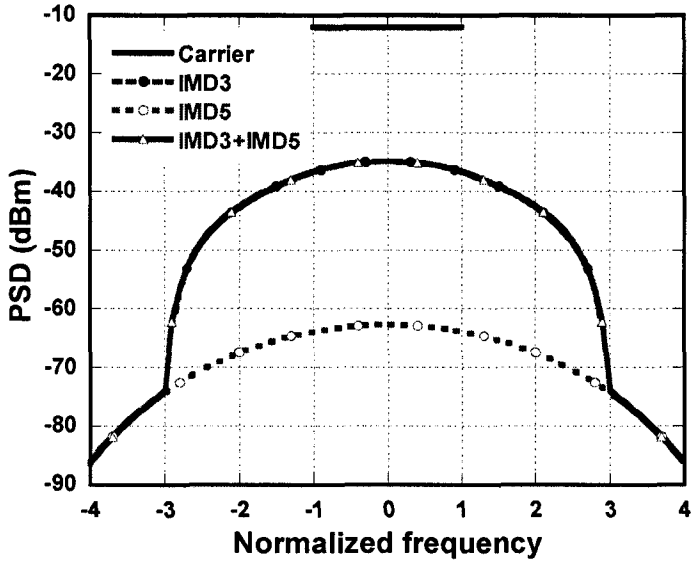

Figure 4.1 Output PSD obtained by using (4.12). $\sigma = 0.15$.

The large bandwidth that the UWB signal covers creates a wide range of potential narrow band interference sources. Both in-band and nearby out-of-band interference sources can cause degradation. The out-of-band power leakage may degrade the adjacent coexisting channel. Adjacent channel power ratio (ACPR) is typically defined as the ratio of the power leakage in a bandwidth of the adjacent bands to the power in the bandwidth within the main signal [28]. ACPR should stay below the value of -20 dB as specified in ECMA-368 [2]. In our system model, the first and second ACPR can be described, respectively,

$$ACPR[1](\sigma) = \frac{2d_1 \int_1^3 s_1(v)dv + 2d_2 \int_1^3 s_2(v)dv}{d_0 \int_{-1}^{1} s_0(v)dv} \tag{4.13a}$$

and $$ACPR[2](\sigma) = \frac{2d_1 \int_3^5 s_1(v)dv + 2d_2 \int_3^5 s_2(v)dv}{d_0 \int_{-1}^{1} s_0(v)dv} \tag{4.13b}$$

where [-1, 1] is the desired in-band, [±1, ±3] is the first adjacent band and [±3, ±5] is the second adjacent band, with equal spectral width. $d_k s_k(v)$ is the PSD of the $(2k+1)^{th}$ order IMD products.

4.2 Impact of Fiber Chromatic Dispersion

In order to investigate the impact of fiber chromatic dispersion, we only consider small signal modulation. Due to chromatic dispersion, the optical carrier and its sidebands are transmitted along the fiber at different velocities. To simplify the expression of the

photocurrent after transmission, we only consider the optical carrier and its first-order sidebands because the higher order sidebands are small enough to be neglected compared with the first-order sidebands. The RF current at ω_{RF} is generated by the beating between the optical carrier at ω_c and both its upper and lower sidebands at $\omega_c \pm \omega_{RF}$.

After transmission over optical fiber of length L and dispersion D, the optical field can be rewritten

$$\begin{aligned} E_{out}(t) &= \left[E_0(t) + E_1(t) + E_{-1}(t)\right] \otimes h_f(t) \\ &= \int_{-\infty}^{\infty} \left[\tilde{E}_0(\omega) + \tilde{E}_1(\omega) + \tilde{E}_{-1}(\omega)\right] \cdot H_f(\omega) \cdot e^{j\omega t} d\omega \end{aligned} \tag{4.14}$$

where $E_0(t)$ is the optical field of the optical carrier, and $E_1(t)$ and $E_{-1}(t)$ are the first-order sidebands, $\tilde{E}_k(\omega)$ is the Fourier transform of $E_k(t)$ (k = 0, 1, -1), $H_f(\omega) = e^{-\frac{\alpha L}{2}} e^{j\frac{L}{v_g}(\omega-\omega_c)} e^{\frac{1}{2}j\beta_2 L(\omega-\omega_c)^2}$ is the fiber transfer function, $\omega_c = 2\pi f_c$, and v_g and $\beta_2 = -\lambda^2 D/(2\pi c)$ are group velocity and group velocity dispersion coefficient of the fiber, respectively.

The Fourier transform of $x(t)$ can be expressed for one OFDM symbol period as $\tilde{X}(\omega) = \sum_{n=-N_{ST}/2}^{N_{ST}/2} X_n \delta(\omega - n\Delta\omega) e^{j(-n\Delta\omega T_{CP} + \varphi_n)}$, where $\Delta\omega$ is subcarrier frequency spacing and φ_n is the RF phase noise at the n^{th} subcarrier (assumed to be Gaussian distributed random variable). After photodetection, the received k^{th} OFDM symbol can be written as

$$y_k(t) \propto \sum_{n=-N_{ST}/2}^{N_{ST}/2} \mathrm{Re}\left\{ Y_n \cdot e^{j\left[(n\Delta\omega+\omega_{RF})\left(t+\frac{L}{v_g}\right)+n\Delta\omega\left(\frac{L}{v_g}-T_{CP}\right)\right]} \right\} \tag{4.15}$$

where $Y_n = \cos(\beta_2 L \omega_{RF} \Delta\omega) X_n e^{j\varphi_n}$ is the normalized received symbol corresponding to the transmitted symbol $X_n = |C_n| e^{j\theta_n}$ at the n^{th} subcarrier. Assuming that constant delay will be compensated by cyclic prefix, after equalization the error vector magnitude (EVM) can be approximated using [34]

$$\begin{aligned} EVM_0{}^2 &= \frac{1}{N_{ST}} \sum_{n=-N_{ST}/2}^{N_{ST}/2} |Y_n - X_n|^2 \\ &= \frac{2}{N_{ST}} \sum_{n=-N_{ST}/2}^{N_{ST}/2} |X_n|^2 \left[1 - \cos(n\beta_2 L \omega_{RF} \Delta\omega + \varphi_n)\right] \\ &\quad - \frac{1}{2N_{ST}} \sum_{n=-N_{ST}/2}^{N_{ST}/2} |X_n|^2 \left[1 - \cos(2n\beta_2 L \omega_{RF} \Delta\omega)\right] \end{aligned} \tag{4.16}$$

Using the following identities $\frac{1}{N} \sum_{n=-N}^{N} e^{jn\theta} = \frac{1}{N} \frac{e^{jN\theta} - 1}{e^{j\theta} - 1} = e^{j(N+1)\frac{\theta}{2}} \cdot \text{sinc}\left(\text{N}\frac{\theta}{2}\right) \Big/ \text{sinc}\left(\frac{\theta}{2}\right)$ and $\int_{-\infty}^{\infty} \cos\varphi_n \frac{1}{\sqrt{2\pi}\sigma_\varphi} e^{\frac{\varphi_k^2}{2\sigma_\varphi^2}} d\varphi_n = e^{\frac{\sigma_\varphi^2}{2}}$, where $|X_n|$ and φ_n are independent identically Gaussian distributed random variables. Averaging EVM_0, we get

$$\begin{aligned} &\left\langle EVM_0{}^2 \right\rangle \\ &= 2 \left(\begin{array}{l} 1 - \exp(-\frac{1}{2}\sigma_\varphi{}^2) \cos\left(\frac{1}{4}(N_{ST}+2)\beta_2 L \omega_{RF} \Delta\omega\right) \\ \times \text{sinc}\left(\frac{1}{4} N_{ST} \beta_2 L \omega_{RF} \Delta\omega\right) \Big/ \text{sinc}\left(\frac{1}{2}\beta_2 L \omega_{RF} \Delta\omega\right) \end{array} \right) \\ &\quad - \frac{1}{2} \left(\begin{array}{l} 1 - \cos\left(\frac{1}{2}(N_{ST}+2)\beta_2 L \omega_{RF} \Delta\omega\right) \\ \times \text{sinc}\left(\frac{1}{2} N_{ST} \beta_2 L \omega_{RF} \Delta\omega\right) \Big/ \text{sinc}\left(\beta_2 L \omega_{RF} \Delta\omega\right) \end{array} \right) \end{aligned} \tag{4.17}$$

Eq. (4.17) shows that the EVM will be degraded by RF carrier phase noise and fiber chromatic distortion. RF carrier phase noise will introduce phase noise in the OFDM subcarriers, and fiber chromatic dispersion will introduce an amplitude distortion in the OFDM subcarriers (as seen by (4.15)). For short range of optical fiber transmission and relatively low RF, the power fading in the OFDM RF subcarriers is negligible, and only RF carrier phase noise has an impact on the EVM_0. For a long optical fiber transmission, the relative intensity noise (RIN) due to phase noise to intensity noise conversion by fiber chromatic dispersion has a big impact [35]. The relative intensity noise due to fiber dispersion for the EML linewidth of $\Delta\omega/(2\pi)$ (=14 MHz at 1547.39 nm for our EML used) can be calculated by [35]

$$RIN(L) = RIN(0) + \frac{1}{\Omega_u - \Omega_l}\int_{\Omega_l}^{\Omega_u} \frac{8\Delta\omega}{\Omega^2}\sin^2\left(\frac{1}{2}\beta_2 L\Omega^2\right)d\Omega \tag{4.18}$$

where $(\Omega_u - \Omega_l)/2\pi = B$ is the signal occupied bandwidth, L is the fiber length and $RIN(0) = -150$ dB/Hz is the laser intrinsic RIN.

4.3 Calculation of EVM

The ultimate goal of our analysis is to obtain measures of EVM degradation due to nonlinear distortion. This can be done by evaluating the signal to noise ratio (SNR). The effective system SNR is defined as the ratio of signal power to total noise power including the power of the in-band distortion terms. It can be expressed in terms of the PSD's of the uncorrelated output components as

$$SNR = \frac{\int_{-B/2}^{B/2} S_u(f)df}{N_0 + \int_{-B/2}^{B/2} S_d(f)df} \tag{4.19}$$

where $S_u(f) = d_0 s_0(f)$ means the PSD of UWB signal, $S_d(f)$ represents PSD of the distortion components given by $S_y(f) - S_u(f)$ using (4.12). B is the bandwidth of the input signal. Because no optical amplification is used, N_0 is the noise contribution from only optical transmitter and receiver electronic noise, and this is called "back-to-back" system noise including shot noise, thermal noise, and RIN, which can be expressed as [36]

$$N_0 = \left[G_A RIN \left(\Re P_{opt} + I_d \right)^2 + 2G_A q \left(\Re P_{opt} + I_d \right) + N_{th}^2 \right] B_e,$$

where B_e of 1.8 GHz stands for the equivalent noise bandwidth of optical receiver. The noise consists of contribution of RIN, $G_A RIN \left(\Re P_{opt} + I_d \right)^2 B_e$, shot noise, $2G_A q \left(\Re P_{opt} + I_d \right) B_e$, and thermal noise, $N_{th}^2 B_e$. G_A = 26.87 dB is the RF amplifier gain at the optical receiver. P_{opt} is the received optical power. q is the electron charge, and I_d = 100 nA is the dark current. The variance of thermal noise is given as $N_{th}^2 = 4k_B T F_n B_e / R_L$, where $k_B = 1.38 \times 10^{-23}$ J/K is the Boltzman constant, and F_n = 3.19 dB is noise figure of the RF amplifier at the receiver, T is the room temperature in Kelvin, and $R_L = 50\Omega$ is the load resistance. These parameters are obtained from the later experiment.

The effective SNR determines ultimately the EVM. The total EVM can be expressed as [37]

$$EVM^2 = \left\langle EVM_0^2 \right\rangle + 1/SNR \tag{4.20}$$

where EVM_0 is given by (4.17).

4.4 Summary

In this chapter, the theoretical analyses is carried out considering carrier phase noise and fiber chromatic dispersion effect on each of the OFDM subcarriers within one symbol. The chapter also presents a simple approximation of the OFDM signal to derive a closed-form expression for the output spectrum. The calculation of EVM for transmission through optical fiber using EML is given.

Chapter 5 Experimental Results and Discussion

In this chapter the experimental setup is described. Then the third-order intermodulation distortion is measured and compared to theoretical results. Finally, we measure the performance of MB-OFDM UWB and investigate the impact of fiber dispersion and optical modulation and analyze the nonlinearities effect on system performance.

5.1 Experimental System Configuration

The considered system setup for the performance evaluation of UWB over fiber and two-tone test are shown in Fig. 5.1.

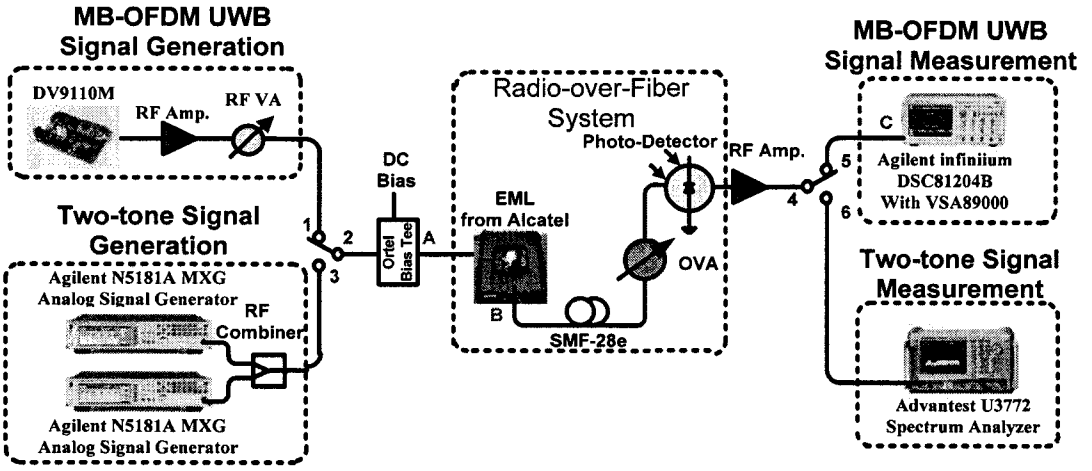

Figure 5.1 Experiment setup for MB-OFDM UWB over fiber system using EML and tow-tone test. RF VA: RF Variable Attenuator, EML: Electro-absorption Modulator integrated laser and OVA: Optical Variable Attenuator.

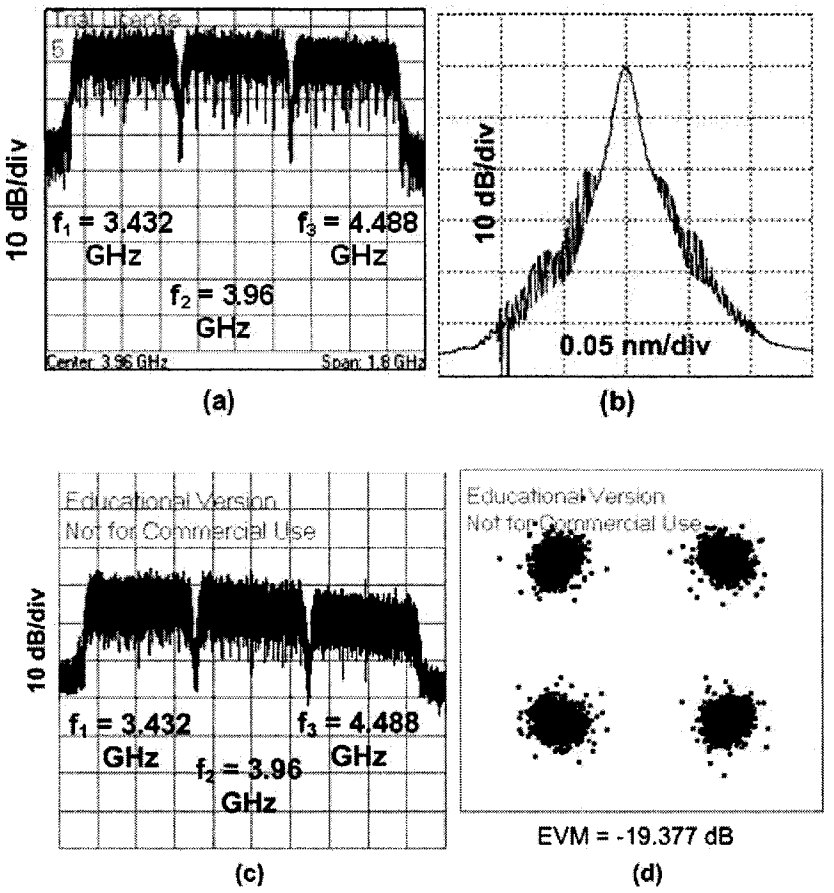

Figure 5.2 (a), (b), (c) and (d) represent the measured RF spectrum at the output from the UWB transmitter (point A), optical spectrum at the output of the EML (point B), RF spectrum and constellation diagram measured by the real time scope (point C) after 40 km of fiber transmission, respectively.

For the performance of MB-OFDM UWB measurement, a commercially available evaluation board, DV 9110M, from WisAir, providing MB-OFDM compliant modulation with three WiMedia subbands allocated at center frequency of f_1 = 3.432, f_2 = 3.96 and f_3 = 4.488 GHz shown in Fig. 5.2 (a), is used for MB-OFDM UWB generation. The bit rate of 200 Mb/s is used for each band with QPSK modulations as shown in Fig. 5.2 (d).

Fig. 5.2 (c) and Fig. 5.2 (d) show the RF spectrum and constellation diagram measured by the real time scope after 40 km of fiber transmission, respectively.

The RF signal is amplified by a broadband RF amplifier from MiniCircuit (ZVA-213) with a low noise figure of 2.6 dB and variable RF attenuator (RF VA) is used to vary the RF power. The UWB signal from the output of the DV9110M Tx module is sent into a 10 Gbit/s digital laser module with integrated electro-absorption modulator from Alcatel. The modulated lightwave is sent through single mode fiber (SMF), with fiber loss of α = 0.21 dB/km and chromatic dispersion of D = 17 ps/(nm.km). We consider UWB over fiber with back-to-back, 20 and 40 km of fiber transmission. An optical variable attenuator (OVA) is used before the photodetector to keep a constant optical signal to noise ratio (OSNR) with constant input optical power to the photodetector and take into account fiber dispersion rather than optical fiber loss. After photodetection, the UWB signal is amplified by a broadband RF amplifier from MiniCircuit (ZVA-213). The photodetector is a high speed photodiode (Discovery DSC-740) with 3 dB bandwidth of 35 GHz, 10 dBm optical power saturation and responsivity of 0.62 A/W. The broadband photodetector combined with the broadband RF amplifier does not introduce amplitude or phase distortion to the OFDM signal, and will be considered as "ideal" optical receiver. The received signal is evaluated with a high speed real time oscilloscope DSO 81204B from Agilent Technologies.

In the two-tone test setup, the RF tones are generated by N5181A MXG RF analog signal generator from Agilent Technologies and the modulated lightwave is sent with back-to-back transmission. The received signal is evaluated with an Advantest U3772 spectrum analyzer.

Optical receiver impact on UWB signal will not be considered in this paper because the optical receiver used is broadband and has a flat magnitude response and constant group delay over the considered signal bandwidth.

5.2 Impact of Bias Voltage of EAM

In order to determine the impact of EML's bias voltage on in-band distortion, we did a two-tone test for back-to-back transmission. We connect point 2 to point 3 and point 4 to point 6 as shown in Fig. 5.1. In the two-tone test, two in-band harmonic signals are applied to the system and the third order intermodulation product is measured versus bias voltage of EML. We measured the difference in dB between the power level of the fundamental carriers and the third-order intermodulation distortion (IMD3) versus bias voltage in the two-tone experiment using RF tones at 3.960 and 3.964 GHz. The RF input power to the EML and the wavelength are 4 dBm and 1547.39 nm, respectively.

We also used the transfer function found in Section III and implemented the simulation of two-tone test in Agilent Advanced Design System (ADS). In this simulation, two tones are supplied at the RF port of the EML. Fig. 5.3 shows measured and simulated power of the fundamental and IMD3 to carrier ratio as a function of EML bias for 4 dBm modulation power of each carrier with a laser bias current of 80 mA at 25 °C. A good agreement between the measured and simulated results is obtained for two-tone test. However, there is discrepancy at low bias voltage of the EML, this is because the transfer function extracted from DC measurement in the range of 0 to 3 V, when the

voltage of the RF signal plus the DC out of this range the model of transfer function is no longer valid. This is the case the bias voltage of the EML near 0 V. We also observe that dips are around 0.25 V and 1.5 V in the measured IMD3 results are different from the simulated IMD3 dips of 0.36 V and 1.44 V using transfer function of the EML. This phenomenon is verified in [38] that the transfer function for an EML cannot represent the insignificant change of the transfer curve of the devices, which results in the change of the IMD3.

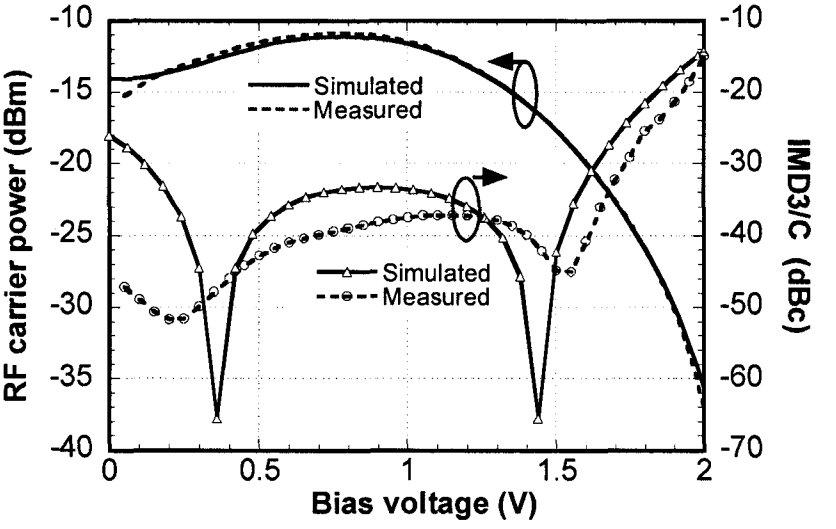

Figure 5.3 Simulated and measured carrier power and IMD3/C versus bias voltage of the EML. Input power is 4 dBm per RF tone.

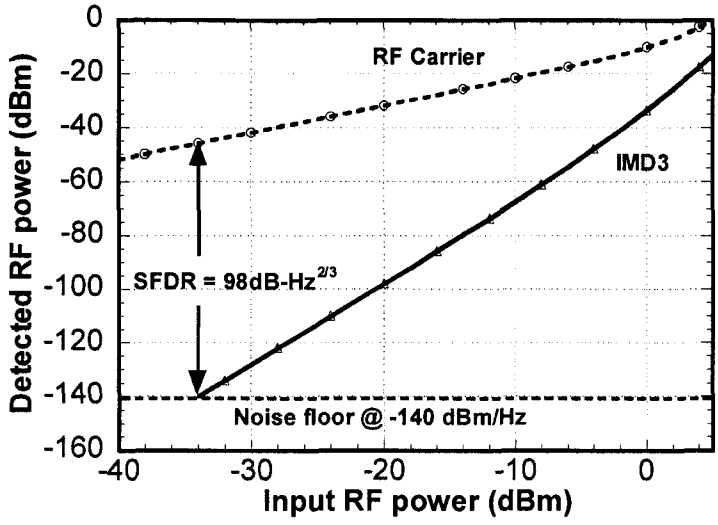

Figure 5.4 RF carrier and IMD3 power versus input RF power for back-to-back transmission. The bias voltage of the EML is 0.26 V.

Next, we set the bias voltage of the EML to 0.26 V and vary the input power per RF tone from -40 to 5 dBm, and simulated the power level of the carrier and IMD3. Fig. 5.4 shows the SFDR is 98 $dB \cdot Hz^{2/3}$ for back-to-back transmission, which meets the SFDR requirement for RoF systems (around 90 $dB \cdot Hz^{2/3}$) [39].

5.3 Effect of Laser Bias Current

Using the setup shown in Fig. 5.1, we connected point 1 to point 2 and point 4 to point 5 and measured EVM versus the bias voltage of the EML at bias current of 40, 80 and 100 mA as shown in Fig. 5.4. The results show that the EVM decreases as the bias voltage increases. This is because IMD3/C and the optical insertion loss increase, as shown in

Fig. 5.3 and Fig. 3.5, respectively. It can be observed from Fig. 5.4 that for the Laser current of 80 and 100 mA, the EVM is almost the same when the bias voltage of EML is lower than 1.7 V, and better than Laser current of 40 mA. The best EVM performances are -21.1 dB, -22.8 dB and -22.8 dB at 0.3 V for bias current of 40, 80 and 100 mA, respectively. The required EVM of -14 dB for data rate of 200 Mb/s, as specified by ECMA-368 [2], is satisfied for a reverse bias voltage of less than 1.42 V, 1.89 V and 1.98 Vat the Laser bias current of 40, 80 and 100 mA, respectively.

Next, we set the bias voltage of the EML to 0.26 V and investigate how the EVM is impacted by the laser bias current. Fig. 5.5 shows the EVM performance at different Laser bias current. It is observed that the EVM is higher than -14 dB when the laser bias current is less than 32.5 mA, improves with the increase of laser bias current and remains almost constant for laser bias current of greater than 50 mA. As we can see from the curve at temperature of 25 °C from Fig. 3.4 (a), the output power of the laser is increased as the laser current increases. By increasing the laser optical power, the EVM drops and improve the performance of RoF system. The EVM decreases until it is saturated at around -22.8 dB due to intrinsic EVM from the source (~ -23 dB).

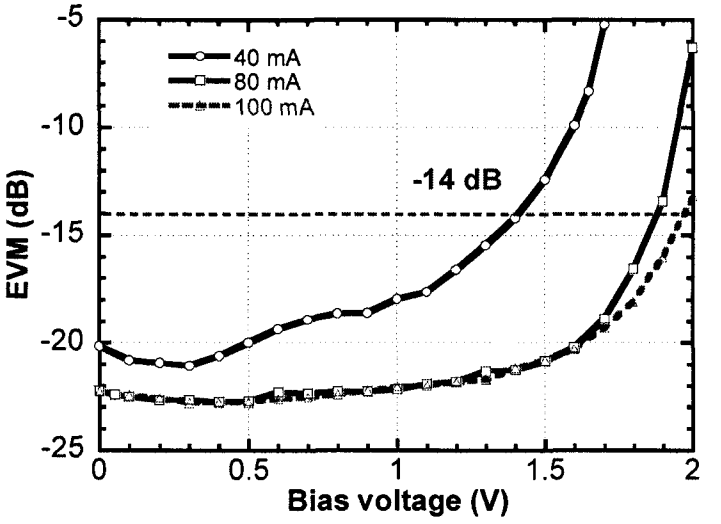

Figure 5.5 Measured EVM versus the bias voltage of the EML at back to back transmission at laser bias current of 40, 80 and 100 mA. The RF input power is 1.3 dBm at 25 °C.

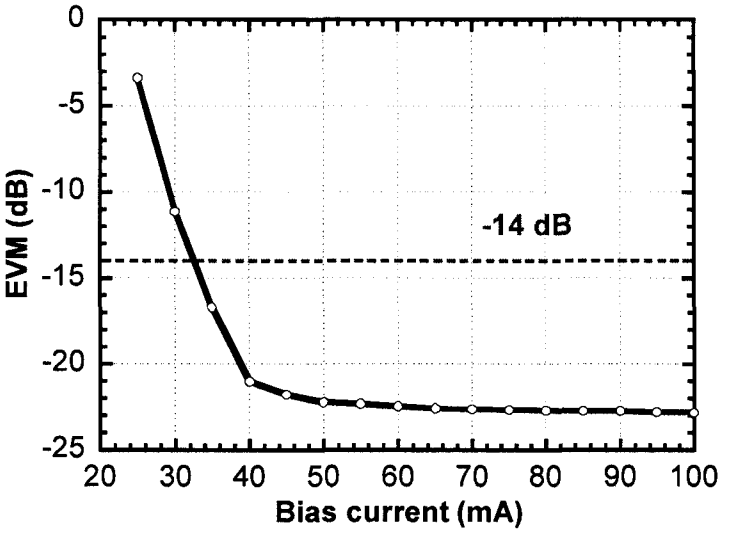

Figure 5.6 Measured EVM versus laser bias current at back to back transmission. The RF input power is 1.3 dBm and the bias voltage of EML is 0.3 V at 25 °C.

The EVM versus bias voltage can be calculated using (4.20) as shown in Fig. 5.6. A good agreement is obtained between the measured and calculated EVM. But there is discrepancy at low bias voltage of the EML because of the transfer function is not valid when bias voltage is near 0 V.

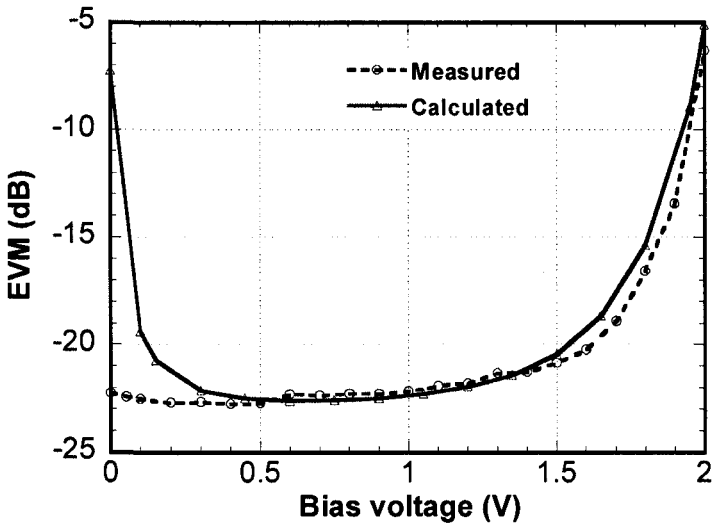

Figure 5.7 Measured and calculated EVM versus bias voltage at back to back transmission. The bias current is 80 mA.

5.4 Effects of Temperature

In order to investigate the effect of EML temperature on the EVM performance, we set the laser bias current to 80 mA and measured EVM at different temperatures. Fig. 5.7 (a) and (b) shows the measured EVM versus bias voltage of the EML at back to back and after 20 km of fiber transmission, respectively, at 25 °C and 50 °C. It can be observed

from both figures that the EVM is better at 25 °C than at 50 °C for different bias voltage. For back-to-back transmission, an EVM of less than -14 dB is achieved at reverse bias voltage of less than 1.16, 1.57 and 1.89 V for 25, 30 and 50 °C, respectively. After 20 km of fiber transmission the EVM degrades and is less than -14 dB at reverse bias voltage of less than 0.98, 1.53 and 1.83 V for 25, 35 and 50 °C, respectively.

From these two figures we can observe that EVM is sensitive to temperature, and the best EVM performance can be obtained at lower temperature. This can be explained, as shown in Fig.3.4 (a), that higher temperature leads to lower output power and thus higher RIN, and also higher nonlinearities of the EML response. The impact of fiber chromatic dispersion will be discussed later.

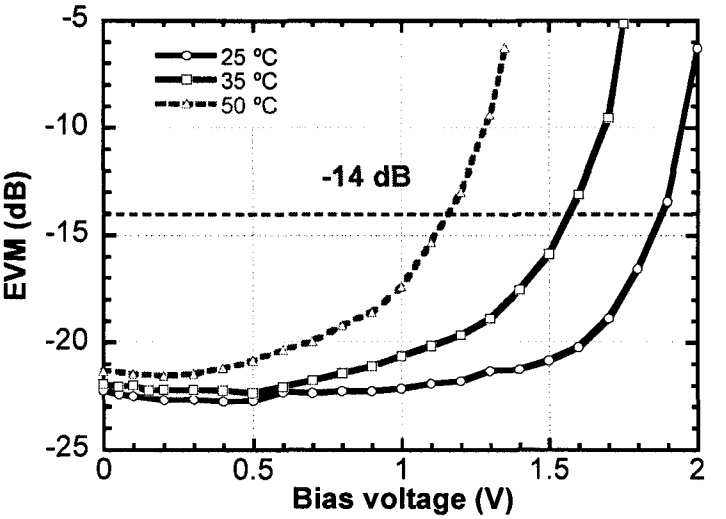

(a)

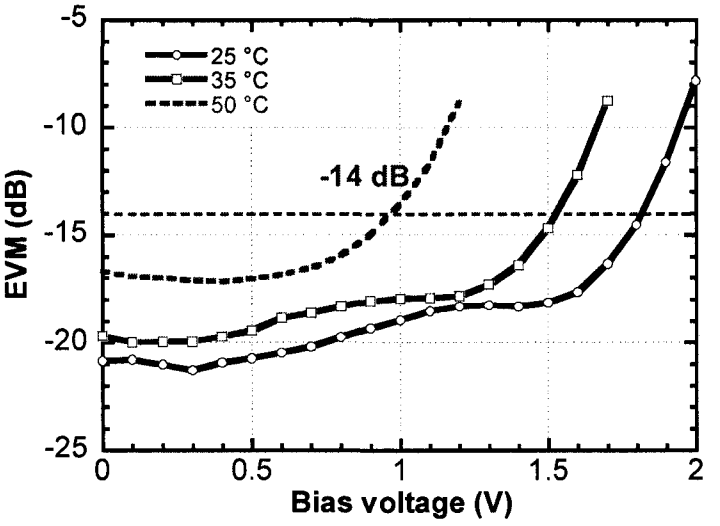

(b)

Figure 5.8 Measured EVM versus bias voltage of the EML (a) at back-to-back and (b) after 20 km fiber transmission at 25 °C, 35 °C and 50 °C. The laser bias current and RF input power are 80 mA and 1.3 dBm, respectively.

5.5 Impact of Optical Modulation

We experimentally characterize the impact of optical modulation and fiber transmission using measured EVM. We set the bias voltage at 0.26 V in the following experiments. For different fiber lengths, we adjust the optical attenuator to keep the same input power to the photodiode. Fig. 5.8 shows measured EVM with normalized input power for back to back and after 20 and 40 km of fiber transmission. The normalized input (modulation) power is defined as $P_{avg} = 2\sigma^2 = \frac{1}{2} V_{rms}{}^2 = V_{RF}{}^2$. It is found that as the normalized input power increases, the EVM decreases and reaches its minimum value of -22.8 dB and then increases. The optimum EVM performance is obtained at normalized power of 0.06~0.07.

In addition, for 20 km and 40 km of fiber transmission, there is 1.5-dB and 3.4-dB EVM degradation, respectively.

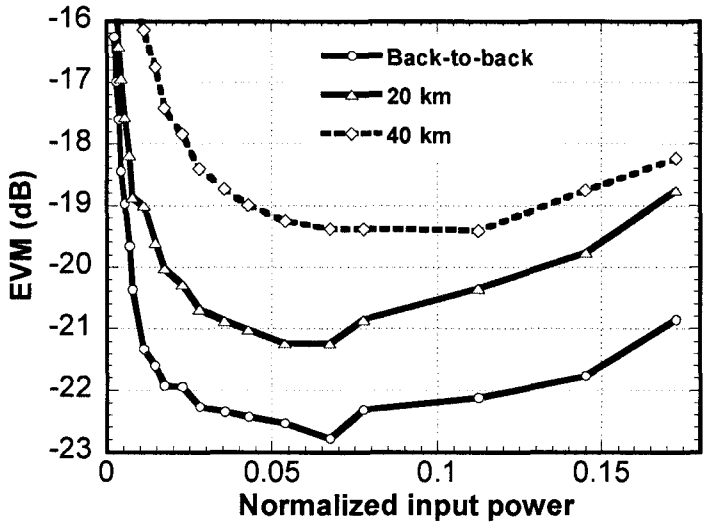

Figure 5.9 Measured EVM versus normalized input power at back to back and after 20 and 40 km of fiber transmission. The bias voltage used is 0.26 V.

OFDM signal has a drawback of a high peak to average power ratio (PAPR). This high PAPR takes place due to parallel processing of a number of data when using a fast Fourier transform (FFT) processor. Nonlinear distortion for the UWB signal can be induced by RF amplifier due to large PAPR, phase noise of the RF carrier local oscillator due to PM to AM conversion and nonlinear response of the EML and fiber chromatic dispersion. Because the high PAPR occurs at low probability [40], the RF amplifier is operated in the linear region for most of the time due to low average power spectral density of the UWB. To distinguish the impact of the EML response nonlinearities and

fiber dispersion, we first consider the back to back UWB over fiber. We can compute the power of IMD products in the received OFDM signal by using (4.10), (4.11) and (4.12). Fig. 5.9 (a) shows calculated power of UWB carrier and sum of IMD3 and IMD5 products. It is seen that with the increase of modulation power, the UWB carrier and IMD3 and IMD5 power increase, and eventually the power of IMD3 and IMD5 is higher than the UWB carrier. This is exactly corresponding to Fig. 5.8 in which EVM decreases and then increases slightly with the increase of modulation power. In addition, the first and second ACPRs are plotted in Fig. 5.9 (b). From this figure, we can observe that for normalized input power of 0 ~ 0.18, ACPRs are below -20 dBc as required by ECMA standard [2]. This means that UWB over fiber using EML can be optimized in terms of EVM and in the meantime the required ACPR can be satisfied.

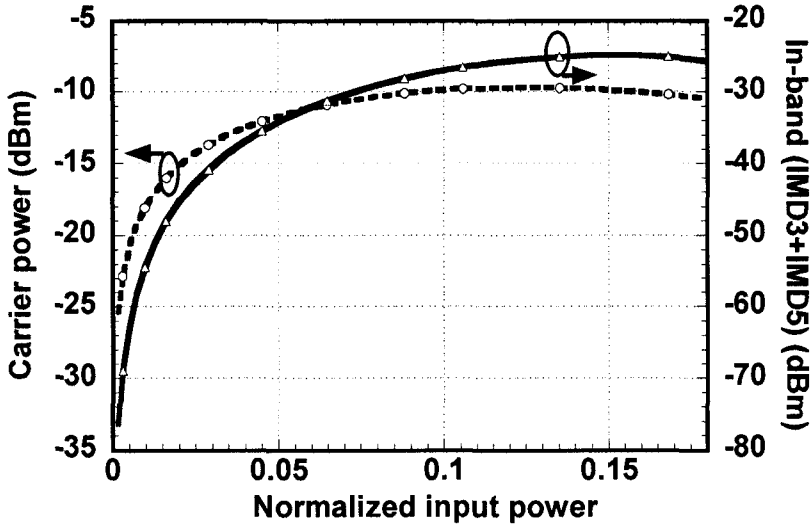

(a)

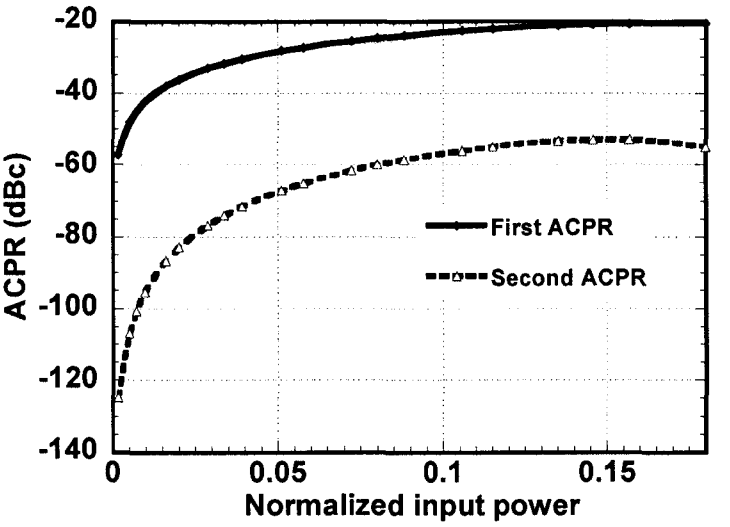

(b)

Figure 5.10 Calculated (a) carrier and in-band IMD3+IMD5 power, and (b) first and second ACPRs versus normalized input power at bias voltage of 0.26 V.

It can be noted that from Eq. (4.8) that there is a pure AM/AM conversion induced distortion depends only on the total transmitted RF power level at the EML. Fig. 5.11 shows the relative amplitude of the subcarriers at 1, 32, 64, 96, and 128 versus normalized input power at back-to-back and after 20 km of fiber transmission for the second band (centered at 3.96 GHz), calculated by (4.8). It can be seen that the amplitude of subcarriers is increasing with normalized input power of up to ~0.068, and normalized input power of higher than 0.068 will decrease the amplitude. It is shown that the different subcarriers have the different amplitude. Any amplitude mismatch between subcarriers may distort the received constellation and degrade the EVM. However, the EVM is not degraded because of the equalization technique, using pilot tones,

implemented in MB-OFDM UWB receiver [3]. Then the best EVM will be obtained when all subcarriers experiences high gain with low intermodulation distortion. This can be achieved at the normalized input power of ~0.068 as shown in Fig. 5.11. This is in a good agreement with the experimental results shown in Fig. 5.9 where the optimum EVM of -22.8 dB is obtained at normalized input power of ~0.068. Compared to the back-to-back, fiber chromatic dispersion will have very little effect on the amplitude distortion because of the negligible chromatic dispersion induced power fading ($\alpha\cos(\beta_2 L\omega_{RF}\Delta\omega)$) on each OFDM subcarrier. There is no phase shift between subcarriers for any modulation because the chirp of the EML is negligible.

At the very low RF input power, the EVM is degraded due to low SNR. On the other hand, at the high RF input power level the EVM increases due to EML nonlinearities.

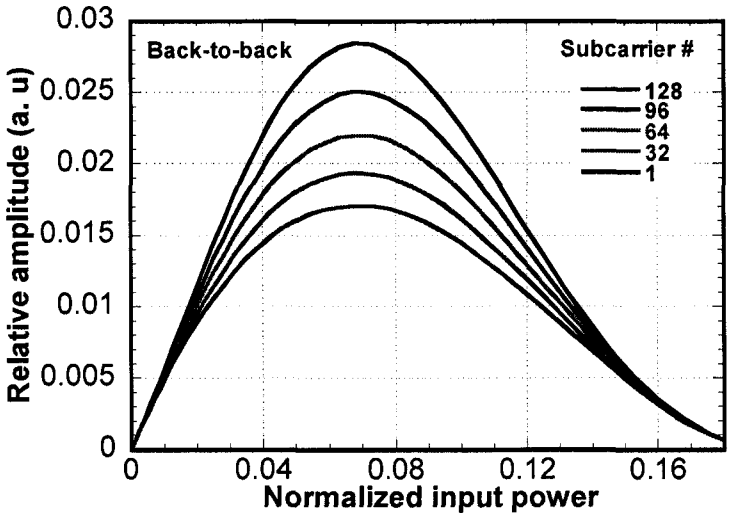

(a)

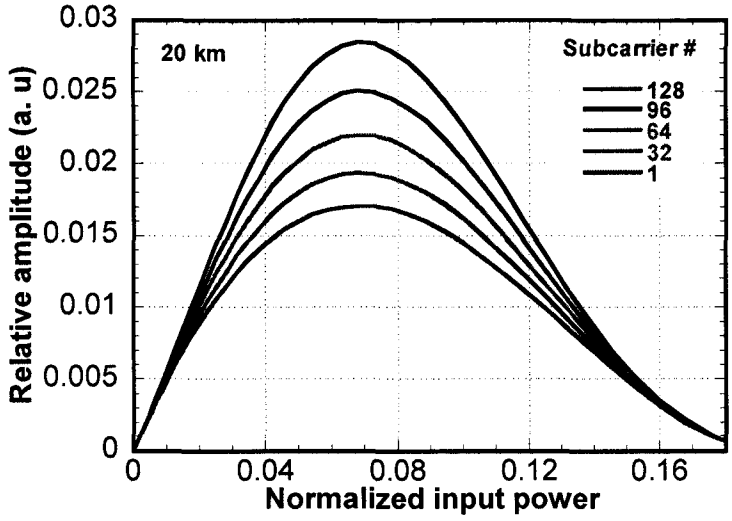

(b)

Figure 5.11 Calculated relative amplitude of subcarriers at 1, 32, 64, 96, and 128 versus normalized input power for UWB over (a) back-to-back fiber and (b) 20 km of fiber transmission.

5.6 Impact of Fiber Transmission

Due to the fiber chromatic dispersion effects, RF power suffers from periodical fading depending on the fiber length L and on the square of the modulation frequency f_c: $P_{RF} \propto \cos^2\left(\frac{D\lambda^2 L\omega_c^2}{2\pi c}\right)$. The normalized received power versus fiber length with λ = 1547.39 nm and D = 17 ps/(nm.km) is shown in Fig. 5.12 for the RF frequency of 3.96 GHz. It can be seen from this figure that after 40 km of fiber transmission, the attenuation is ~0.3 dB. There is less than 3 dB of attenuation when the distance traveled is not more than 120 km.

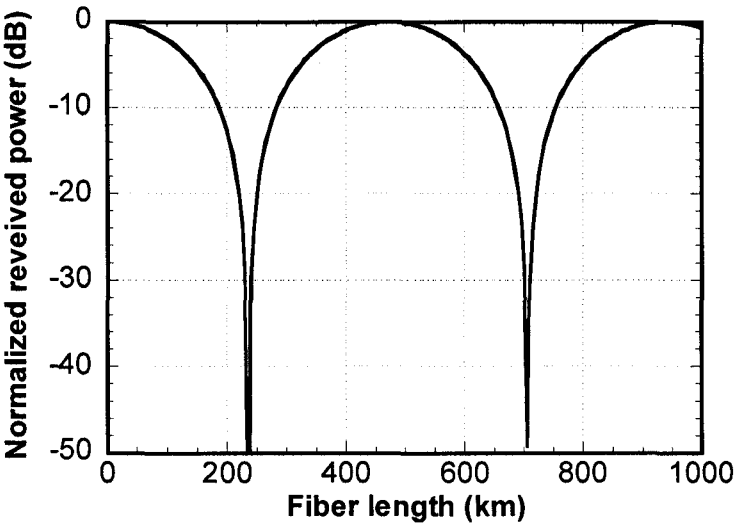

Figure 5.12 Normalized received power versus fiber length for f_c = 3.96 GHz.

Fiber dispersion changes the laser RIN due phase noise to intensity noise conversion [35]. Fig. 5.13 shows total RIN due to fiber dispersion for a laser with linewidth of $\Delta\omega/(2\pi) = 1.4$ MHz at 1547.39 nm by using (4.18), for the frequency band of interest from 3.06 to 4.86 GHz, the dispersion increases the RIN by 5.7 and 10.65 dB for 20 and 40 km, respectively, compared to the back to back. The increase of RIN is due to the interaction of the laser phase noise and chromatic dispersion of the fiber. This is one of the reasons why the EVM degrades with fiber length.

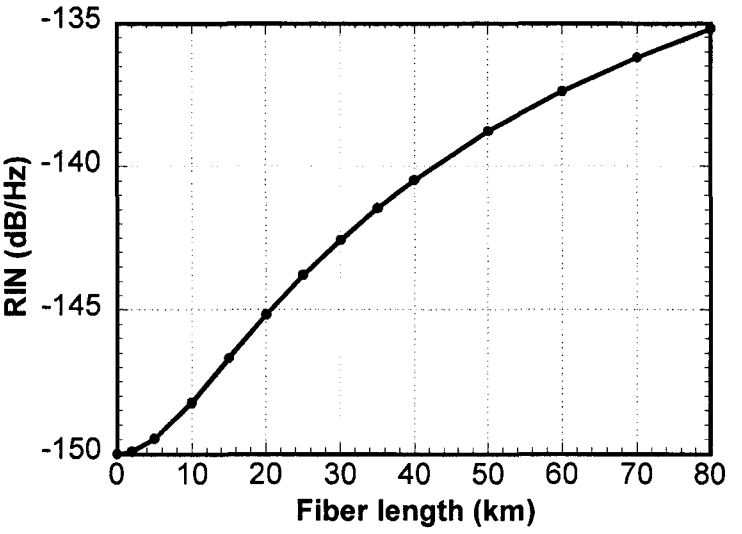

Figure 5.13 Calculated total RIN versus fiber length.

Calculated EVM degradation of the system versus fiber length using (4.18) and (4.19) is shown in Fig. 5.14. In the EVM computation we used intrinsic EVM of -23 dB and SNR computed due to thermal noise only, which gives a phase noise power of σ_{φ}^{2} ~0.005. The EVM degradation is obtained with respect to the back to back at normalized input power of 0.068. Compared to the back to back, it is shown that EVM degradation of ~1.25 dB and ~3.59 dB is expected after 20 and 40 km of fiber transmission, respectively. This is in good agreement with the measurement in Fig. 5.8.

Compared to the back to back, the fiber transmission is mainly limited by laser phase noise converted RIN due to fiber chromatic dispersion.

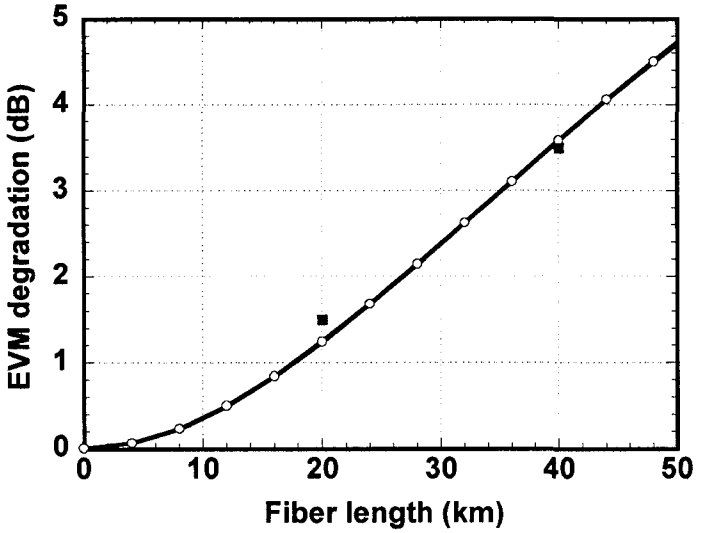

Figure 5.14 Calculated EVM degradation versus fiber length with respect to back to back. Black square: experimental results for fiber length of 20 and 40 km.

5.7 Summary

This chapter presents the experimental setup for the performance evaluation of UWB over fiber system and two-tone test. The performance of UWB over fiber system is clarified with focus on the ECMA-368 standard using MB-OFDM. EVM measurement is carried out to evaluate the system performance considering the effect of fiber length, bias voltage, bias current, temperature, and input RF power of the EML. Optical transmitter's nonlinearities and fiber dispersion effect on system performance are studied experimentally and compared to the theoretical analysis. Good agreement between the experiment results and theoretical analysis is obtained.

Chapter 6 Conclusions

6.1 Summary

In this work, we have experimentally investigated and theoretically analyzed the performance of MB-OFDM UWB signal transmitted over fiber using a low cost EML. EVM is used to evaluate the system quality of UWB signal considering system's parameters such as bias current, temperature, modulation voltage (power) and bias voltage of the EML. The experimental results showed how EVM performance is affected by system's parameters such as bias current, bias voltage and temperature of the EML, and fiber length. General trends were observed that EVM degrades when either EML's bias current decreases or temperature increases or fiber length is longer. Moreover, EVM is sensitive to temperature and not very sensitive to bias current of more than 50 mA. Performance degradation of MB-OFDM UWB over fiber system caused by EML nonlinearities and fiber chromatic dispersion is investigated. The IMD and ACPR are also theoretically analyzed.

It is found that there is a minimum bias current for EML, which depends on temperature. For the considered EML, the minimum bias current is 80 mA at 25 °C. Also there is optimum modulation voltage (or power) at given bias voltage. For this EML, the optimum normalized input (modulation) power is ~0.068 at bias voltage of 0.26 V. When modulation voltage is low the performance is mainly limited by signal to noise ratio, but mainly limited by EML response nonlinearities when modulation power is high.

Moreover, when the optimum normalized input power is used fiber transmission is further limited by laser phase noise converted RIN due to fiber dispersion in addition to increase of optical amplifier noise due to fiber loss, compared to back to back UWB over fiber. The performance of MB-OFDM UWB is mainly limited by laser phase noise converted RIN considering system's parameters such as linewidth and fiber transmission length. It is shown using a narrow linewidth laser with low RIN will significantly improve system performance.

6.2 Future Works

MB-OFDM UWB over fiber is a fast emerging technology. There are still many areas of UWB over fiber are yet to be explored. The following is the suggestions for future work.

- The phase shifts between subcarriers are not considered in this thesis. The phase shifts between subcarriers can be obtained by measuring the chirp parameter of the EML.
- Investigating the performance of MB-OFDM UWB over fiber transmission by using laser direct modulation can be done.
- Wavelength division multiplexing (WDM) UWB over fiber system can be studied in the future.

References

[1] Revision of Part 15 of the Commission's Rules regarding ultra-wideband transmission system first report and order federal communications commission, 2002, ET-Docket 98–153, FCC02–48.

[2] ECMA-368, High rate ultra wideband PHY and MAC standard, ECMA International, Geneva, 2nd edition, Dec. 2007.

[3] "Multi-band OFDM physical layer proposal for IEEE 802.15 task group 3a", IEEE 802.15 Working Group for WPAN, March 2004.

[4] A. J. Cooper, "Fiber/radio for the provision of cordless/mobile telephony services in the access network," Electron. Lett., vol. 26, no. 24, pp. 2054-2056, Nov. 1990.

[5] D. K. Mynbaev, L. L. Scheiner, "Fiber optic communications technology", (Prentice Hall, New Jersey, 2001).

[6] J. Capmany, B. Ortega, D. Pastor, and S. Sales, "Discrete-time optical processing of Microwave Signals", J. Lightwave Technol., Vol. 23, No. 2, 703 - 723, (2005).

[7] H. Al-Raweshidy, "Radio over fibre technology for the next generation" in *Radio over Fiber Technologies for Mobile Communications Networks"*, H. Al-Raweshidy, and S. Komaki, ed. (Artech House, Inc, USA, 2002).

[8] H. Bong Kim and A. Wolisz, "A radio over fiber based wireless access network architecture for rural area," 14th IST Mobile and Wireless Commun. Summit, Dresden, June 2005.

[9] Y. Cheng, Y. Lin, M. Wang, F. Cheng, C. Wu and Y. Yu, "Integrated a hybrid CATV/GPON transport system based on 1.31/1.49/1.55 μm WDM transceiver module," QELS' 05: Quantum Electron. Laser Sci. Conf. vol 3, pp 1678-80.

[10] M. Ran, Y. Ezra, M. Haridim, and B. Lembrikov, "Ultra wideband radio over optical fiber," Wireless Word research forum, White Paper V1.21 March 2007.

[11] C.M. Tan, L.C. Ong, M.L. Yee, B. Luo, P.K. Tang, "Direct yransmission of ultra wideband signals using single mode radio-over-fiber System", Asia-Pacific Microwave Conference, Dec 2005.

[12] S. Kim, H. Jang, S, Choi, Y. Kim, J, Jeong, "Performance evaluation for UWB signal transmission with different modulation schemes in multi-cell environment distributed using RoF technology", Joint Intl Workshop on UWBST & IWUWBS, pp. 187-191, May 2004.

[13] M.Y.W. Chia, M.L Yee, "Wireless ultra wideband communications using radio-over-fiber", IEEE conference on Ultra Wideband Systems & Technologies, pp. 265-269, Nov 2003.

[14] L.C. Ong, M.L. Yee, B. Luo, "Transmission of ultra wideband signals through radio-over-fiber Systems", Proceedings of IEEE Lasers & Electro-Optics Society, pp. 22-523, Oct 2006.

[15] F. Tabatabai, H. Al-Raweshidy, "Performance evaluation for WLAN and UWB using radio over fiber", Proceedings of 9th European Conference on Wireless Technology, pp. 147-149, Sep 2006.

[16] Y. Guennec, M. Lourdiane, B. Cabon, G. Maury, P. Lombard, "Technologies for UWB-over fiber," in Proc. IEEE Lasers and Electro-Optics Society (LEOS) Annual Meeting, pp. 518-519, Oct. 2006.

[17] A. Pizzinat, B. Charbonnier, M. Moignard, "Analysis of laser induced distortions in ultra wide band MB-OFDM over fiber," in Proc. IEEE Lasers and Electro-Optics Society (LEOS) Annual Meeting, pp. 339-340, Oct. 2006.

[18] M. Yee, V. Pham, Y. Guo, L. Ong, B. Luo, "Performance evaluation of MB-OFDM ultra-wideband signals over single mode fiber," in Proc. International Conference on the Ultra Wideband (ICUWB), pp. 674-677, Sep. 2007.

[19] Y. Guo, V. Pham, M. Yee, L. Ong, B. Luo, "Performance study of MB-OFDM ultra-wideband signals over multimode fiber," in Proc. International Conference on the Ultra Wideband (ICUWB), pp. 429-431, Sept. 2007.

[20] M. Yee, V. Pham, Y. Guo, L. Ong, B. Luo, "Performance evaluation of multiband radio-over fiber for WLAN, Gigabit Ethernet and UWB," in Proc. IEEE International Microwave Symposium (IMS), pp. 491-494, Jun. 2008.

[21] M. Yee, Y. Guo, L. Ong, J. Zhu, J. Hao, "Performance evaluation of bidirectional MB-OFDM UWB over cable, MMF and SMF," in Proc. IEEE International Microwave Symposium (IMS), pp. 357-360, 2009.

[22] M. Jazayerifar, B. Cabon, J. Salehi, "Transmission of multi-band OFDM and impulse radio ultra- wideband signals over single mode fiber," J. Lightw. Technol., vol. 26, no. 15, pp. 2594-2603, Aug. 2008.

[23] D. Smith, A. Borghesani, D. Moodie, M. Thakur, T. Quinian, S. Dudley, M. Toycan, C. Bock, S. Walker, M. Ran, Y. Ben-Ezra, "480 Mbps ultra-wideband

radio over fibre transmission using a 1310/1550 nm reflective electro-absorption transducer and off-the-shelf components," in Proc. Optical Fiber Communication Conference and Exposition (OFC) and The National Fiber Optic Engineers Conference (NFOEC), pp. 1-3, Feb. 2008.

[24] M. Sakib, B. Hraimel, X. Zhang, M. Mohamed, W. Jiang, Ke Wu, and D. Shen, "Impact of optical transmission on multiband OFDM ultra-wideband wireless system with fiber distribution," J Lightwave Technol, vol. 27, no. 18, pp. 4112-23, 15 Sept. 2009.

[25] G. F. Ross, "Transmission and reception system for generating and receiving base-band duration pulse signals for short base-band pulse communication system," U.S. patent 3728632, Apr. 17, 1973.

[26] http://www.wimedia.org/en/resources/worldwide_regulatory.asp.

[27] H. Weber and M. Nakazawa, "Ultrahigh-speed optical transmission technology," New York, NY: Springer, 2007.

[28] Adjacent Channel Power Ratio (ACPR) application note, Anritsu Application Note.

[29] G. W. Lee and S. K. Han, Linear dual electroabsorption modulator for analog optical transmission, Microwave Opt Technol Lett 22 (1999), 369-373.

[30] P. Doussière, V. Rodrigues, R. Simes, P. Wolkowicz, "Electroabsorption-modulated DFB laser ready to attack 10Gbit/s market," Alcatel Optronics.

[31] Y. Yu, R. Lewen, U. Westergren, L. Thylen, S. Irmscher and U. Eriksson, "Temperature-dependent effects in high-speed traveling-wave electroabsorption modulators," Electron. Lett., Vol. 41, No. 4, Feb. 2005.

[32] N. Horvath and I. Frigyes, "Effects of the nonlinearity of a Mach-Zehnder modulator on OFDM radio-over-fiber transmission," IEEE Communications Letters, v 9, n 10, p 921-3, Oct. 2005.

[33] P. Banelli and S. Cacopardi, "Theoretical analysis and performance of OFDM signals in nonlinear AWGN channels," IEEE Trans. Commun., vol. 48, pp. 430–441, Mar. 2000.

[34] C. Zhao, R. Baxley, "Error vector magnitude analysis for OFDM systems," in Proc. Asilomar Conference on Signals, Systems, and Computers (ACSSC), pp. 1830-1834, Oct. - Nov. 2006.

[35] W. Marshall, B. Crosignani, A. Yariv, "Laser phase noise to intensity noise conversion by lowest-order group-velocity dispersion in optical fiber: exact theory," Optics Letters, vol. 25, no. 3, pp. 165-167, Feb. 2000.

[36] M. Mohamed, X. Zhang, B. Hriamel, Ke Wu, "Analyssis of frequency quadrupling using a single Mach-Zehnder modulator for millimeter-eave generation and distribution over fiber system," Optics Express, vol. 16, no. 14, Jul. 2008.

[37] A. Georgiadia, "Gain, phase imbalance, and phase noise effects on error vector magnitude," IEEE Trans. On Vehicular Tech, vol. 53, no. 2, pp. 443-449, Mar. 2004.

[38] Y.S. Yun, Y.W. Choi, J.D. Chung and J.H. Kim, "Analog performance of multiple-quantum-well electroabsorption modulation," Optical and Quantum Electronics (2005) 37: 1025-1031.

[39] D. Wake, M. Webster, G. Wimpenny, K. Beacham, and L. Crawford, "Radio over fiber for mobile communications," in 2004 IEEE Int. Topical Meeting Microwave Photonics (MWP 2004), pp. 157–160.

[40] J. Liu, H. Arslan and L. P. Dunleavy, "Effect of power amplifier impairments in designing OFDM based wireless communication systems," IEEE Topical Conference on Wireless Communication Technology, Honolulu, HI, Oct. 15-17, 2003.